Article

Lignin to adipic acid in a high-yield chemical and biological redox process

https://doi.org/10.1038/s41586-026-10580-x

Received: 31 July 2025

Accepted: 21 April 2026

Published online: 10 June 2026

Check for updates

Kathryn M. Mains[1,2,6], Chad T. Palumbo[1,6], Davide Rigo[1,2,6], Matthew S. Webber[1,2,6], Gloria Rosetto[1], Si Tong Bao[1], Austin L. Carroll[2,3], Nicolette R. Meyer[1], Alexander F. Benson[1], Brett A. Boyle[1], Stefan J. Haugen[1], Morgan A. Ingraham[1], William G. Alexander[2,3], Miriam Silberman[3], Logan C. Myers[1], Kelsey J. Ramirez[1], Kevin P. Sullivan[1], Adam M. Guss[2,3], Davinia Salvachúa[1], Yuriy Román-Leshkov[4], Shannon S. Stahl[5]✉, Allison Z. Werner[1,2]✉ & Gregg T. Beckham[1,2]✉

Viable manufacturing pathways to produce bio-based chemicals from renewable feedstocks, such as lignin derived from plant biomass, are needed to decarbonize the chemicals manufacturing sector. Converting the recalcitrant lignin polymer to valuable bioproducts remains a longstanding challenge in biorefining, with the highest reported single-product yield from lignin currently around 20 wt% (refs. 1–4). Most existing lignin depolymerization strategies target aryl–ether bond cleavage, which can produce aromatic monomers in yields of only about 30 wt%, and still as complex mixtures with C–C-linked dimers and oligomers[5,6]. The recalcitrance of these C–C linkages between aromatic moieties fundamentally limits single-product yields from lignin, prompting the development of strategies to efficiently cleave these C–C bonds[3,7–9]. Here we show how reductive processing of lignin from poplar accesses a hydrocarbon mixture of alkyl-aromatic monomers and oligomers that is privileged for oxidative conversion to monomeric aromatic carboxylic acids, comprising mostly benzoic acid and phthalic acid isomers in up to 73 wt% monomer yields, using a Co/Mn/Br catalyst. The soil bacterium *Pseudomonas putida* KT2440 was engineered to convert this mixture of aromatic carboxylic acids to muconolactone, a precursor to bio-based nylons, enabling final adipic acid yields up to 26 wt% (gram adipic acid per gram lignin) with a maximum theoretical yield of 57 wt%. This pairing of reductive and oxidative steps with lignin resembles processes in petrochemical refining and shows how lignin may be converted into a single, valuable bioproduct in high yields.

The petrochemical industry converts aromatic hydrocarbons to valuable chemicals through integrated processes that often include catalytic reductions and oxidations[10,11]. A similar strategy could support efforts to decarbonize chemical manufacturing using renewable feedstocks and biochemical processes, as exemplified in adipic acid production[12] (Fig. 1). Of particular interest from biogenic feedstocks, lignin is an abundant, aromatic plant biopolymer that consists of phenylpropanoid subunits connected by C–O and C–C bonds with varying degrees of aromatic ring methoxylation. Lignin has long been pursued as a source of aromatic compounds[5,13,14], but its heterogeneous composition and chemical reactivity limit its utility as a chemical feedstock. Lignin often degrades during extraction from biomass[5,15], and most methods for lignin depolymerization cleave only C–O bonds, resulting in the formation of complex mixtures of monomeric and oligomeric phenols[5,6]. For these reasons, efforts targeting conversion of lignin to various single products, including benzene, β-ketoadipic acid and 2,6-dimethoxybenzoquinone, have not achieved yields higher than about 20 wt% (gram single product per gram lignin)[1–4]. Methods to cleave C–C bonds could significantly improve lignin utilization[3,7–9], and oxidative processes used in the petrochemical industry offer a potential strategy to achieve this goal. Phenols in the product mixture have antioxidant properties, however, and thus inhibit radical-based oxidation reactions that are often used industrially[5,9,16]. These complications motivated efforts to identify a different strategy to access aromatic building blocks from lignin.

Here we show how the pairing of reduction and oxidation processes overcomes historical limitations in the conversion of lignin to a single product (Fig. 1b). Catalytic hydrodeoxygenation (HDO) converts lignin-derived monomers and oligomers into a mixture of alkyl aromatics that lack inhibitory phenols. Previous studies of HDO with lignin feedstocks have prioritized energy applications[17–19], such as aviation fuel blendstocks, but we anticipated that this hydrocarbon mixture could be a privileged feedstock for catalytic autoxidation to produce performance-advantaged or bioprivileged chemicals[20,21]. Conditions similar to those of the Mid-Century process used industrially to convert *p*-xylene to terephthalic acid[10,22,23] provide a means to convert this

[1]Renewable Resources and Enabling Sciences Center, National Laboratory of the Rockies, Golden, CO, USA. [2]Center for Bioenergy Innovation, Oak Ridge National Laboratory, Oak Ridge, TN, USA. [3]Biosciences Division, Oak Ridge National Laboratory, Oak Ridge, TN, USA. [4]Department of Chemical Engineering, Massachusetts Institute of Technology, Cambridge, MA, USA. [5]Department of Chemistry and Great Lakes Bioenergy Research Center, University of Wisconsin-Madison, Madison, WI, USA. [6]These authors contributed equally: Kathryn M. Mains, Chad T. Palumbo, Davide Rigo, Matthew S. Webber. ✉e-mail: stahl@chem.wisc.edu; allison.werner@nlr.gov; gregg.beckham@nlr.gov

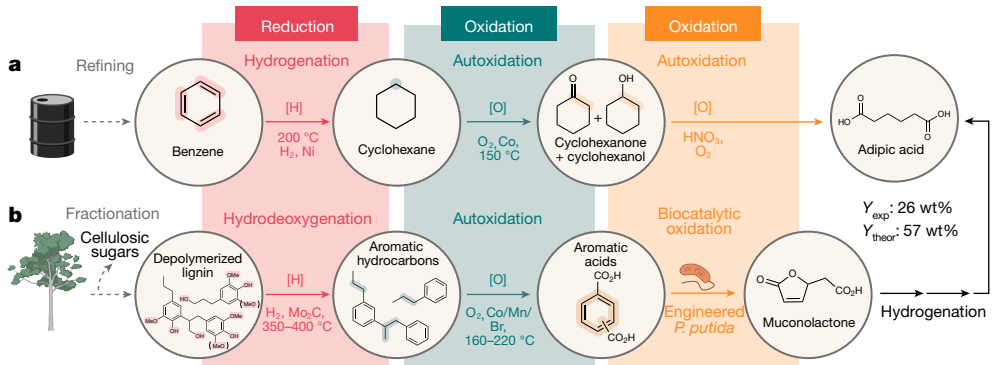

Fig. 1 | Comparison of nylon monomer synthesis through petrochemical routes and from lignin. a, The current manufacturing route for adipic acid proceeds through reduction of petroleum-derived benzene to cyclohexane, oxidation of cyclohexane to cyclohexanone and cyclohexanol (KA oil), followed by nitric acid-mediated oxidation to adipic acid. **b**, Our proposed strategy to produce high-yield, single products from lignin combines extraction and stabilization of lignin from biomass via reductive catalytic fractionation, hydrodeoxygenation of lignin to produce aromatic monomeric and oligomeric hydrocarbons, catalytic autoxidation of the aromatic hydrocarbons to bioavailable monomers, and biological funnelling to produce muconolactone, which can be used to produce monomers for incumbent or performance-advantaged nylons, such as adipic acid via a three-step hydrogenation. The experimental yield (Y_{exp}) for the proposed overall process in **b** was calculated on a weight (wt)% basis, where $Y = \text{mass}_{\text{adipic acid}}/\text{mass}_{\text{biomass lignin}}$. The theoretical product yield, Y_{theor}, for the proposed overall process in **b** was calculated based on a theoretical molar conversion of all reactants to products (assumptions, data and calculations are available in Extended Data Fig. 2, Supplementary Information and Supplementary Data 1). Figure created in BioRender; Mains, K. https://BioRender.com/9hcf8sw (2026).

deoxygenated product stream to aromatic carboxylic acid monomers that could undergo biological funnelling into a single product[24,25]. We validate this hypothesis by optimizing the catalytic oxidation of HDO oil derived from poplar lignin and by engineering a strain of the robust soil bacterium *Pseudomonas putida* KT2440 to maximize conversion of aromatic carboxylic acids to muconolactone. Finally, we hydrogenate muconolactone to produce adipic acid, attaining an overall process yield towards adipic acid of 26 wt% (gram adipic acid per gram lignin) out of a maximum theoretical yield of 57 wt%. This equates to a yield of 6.8 wt% on a total biomass basis. The experimental yield was calculated on a mass basis and the theoretical yield was calculated using the reaction stoichiometries for each process step[20,21,26,27] (Fig. 1b and Extended Data Figs. 1 and 2; the assumptions, data and calculations are available in Supplementary Text and Supplementary Data 1). The sequence of chemical and biological redox steps used in this process establishes a platform for conversion of complex lignin streams into valuable bioproducts[28].

Aromatic carboxylic acids from lignin

Reductive catalytic fractionation (RCF) is an effective strategy to extract lignin from biomass, enabling direct conversion of lignin to a mixture of monomeric and oligomeric phenols while generating a high-quality stream of solid carbohydrate products[1,28]. Here we used a ruthenium (Ru)/carbon (C) catalyst and a 2:1 v/v methanol/water solvent to perform RCF of poplar biomass[1,28] (Supplementary Fig. 1). We generated 300 g of RCF oil over the course of multiple scaled reactions, with small-scale tests at identical conditions achieving RCF oil yields of 74 wt% (Y, where $Y = \text{mass}_{\text{RCF oil}}/\text{mass}_{\text{biomass lignin}}$). The remaining lignin is retained in the carbohydrate pulp. The oil consisted of 42 wt% monomers ($x_{\text{mono}} = \sum\text{mass}_{\text{monomers in product}}/\text{mass}_{\text{product oil}}$), with oligomers comprising the majority of the remaining mass balance (Supplementary Figs. 1–4). Complete cleavage of ether C–O bonds in the RCF oil was confirmed by ^{1}H–^{13}C heteronuclear single quantum coherence (HSQC) nuclear magnetic resonance (NMR) spectroscopy, indicating that the remaining aromatic oligomers are linked by C–C bonds[29] (Supplementary Fig. 3).

We then performed catalytic HDO of the solvent-free RCF oil to generate a hydrocarbon-based mixture by removing the phenol and aromatic methoxyl groups. This step, which used molybdenum carbide (Mo_2C) as a catalyst in a dual-pass flow-through process conducted in a trickle-bed reactor[17,19], produced a deoxygenated lignin oil at a 58 wt% yield (Y, where $Y = \text{mass}_{\text{HDO oil}}/\text{mass}_{\text{RCF oil}}$), equating to a mass yield of 43 wt% on an initial lignin basis ($Y = \sum\text{mass}_{\text{HDO oil}}/\text{mass}_{\text{initial lignin}}$) (Supplementary Fig. 5). Much of the mass loss during HDO can be accounted for by water and methane formation, as well as losses due to laboratory-scale material transfers[17–19]. Analysis of the HDO products by gas chromatography and ^{1}H–^{13}C HSQC NMR spectroscopy (Supplementary Figs. 5–7), showed an aromatic monomer selectivity of 40 wt% ($x_{\text{mono}} = \sum\text{mass}_{\text{aromatic monomers in product}}/\text{mass}_{\text{product oil}}$), with the monomers primarily consisting of propylbenzene and methyl propylbenzene isomers[30] (Supplementary Fig. 5).

We subsequently evaluated the poplar-derived HDO oil as a substrate for catalytic autoxidation (Fig. 2 and Supplementary Figs. 8–14), using a Co/Mn/Br catalyst system in acetic acid (AcOH), similar to that used for industrial conversion of *p*-xylene to terephthalic acid[12,26]. We used the following catalyst composition as the baseline condition for these optimization studies: $Co(OAc)_2{\cdot}4H_2O$, $Mn(OAc)_2{\cdot}4H_2O$ and NaBr at 5 wt%, 5 wt% and 0.5 wt%, respectively (Fig. 2a). Reactions were performed for 1 h at 160 °C with 6 bar O_2. The product mixture obtained under these conditions was rich in benzoic acid and the three benzene dicarboxylic acid isomers, with minor amounts of benzene tricarboxylic acids and biphenyl-3,3′-dicarboxylic acid. Assessment of the different variables (co-catalyst loading, reaction time, temperature and O_2 partial pressure) was done in batch reactors (Fig. 2a and Supplementary Fig. 8) and led to the following optimized conditions: 5% $Co(OAc)_2{\cdot}4H_2O$, 5% $Mn(OAc)_2{\cdot}4H_2O$ and 1% NaBr (all loadings in wt% relative to the substrate) for 3 h at 220 °C and 6 bar O_2. A small increase in monomer yields was obtained by increasing the substrate loading from 2.5 g l^{-1} to 25 g l^{-1} (Supplementary Fig. 9), beyond which we observed stoichiometric O_2 limitations imposed by using batch reactors (Supplementary Text)—a limitation that could be overcome in a scaled process using a continuous reactor, as is practiced commercially for terephthalic acid production[31,32].

To better understand the effect of aromatic substitution on the autoxidation reaction, we next examined the reactivity of alkyl-aromatic monomers and dimers present or resembling fragments in HDO oil under optimized conditions (Fig. 2b and Supplementary Fig. 10), owing to the fact that varying alkyl constituents can have a substantial role in oxidation reaction outcomes[22]. Propylbenzene, the major monomer present in HDO oil, undergoes oxidative C–C cleavage to afford benzoic acid in 93 mol% yield, while showing little variation with respect to yield at solvent water concentrations up to 25 vol% (Supplementary Fig. 11).

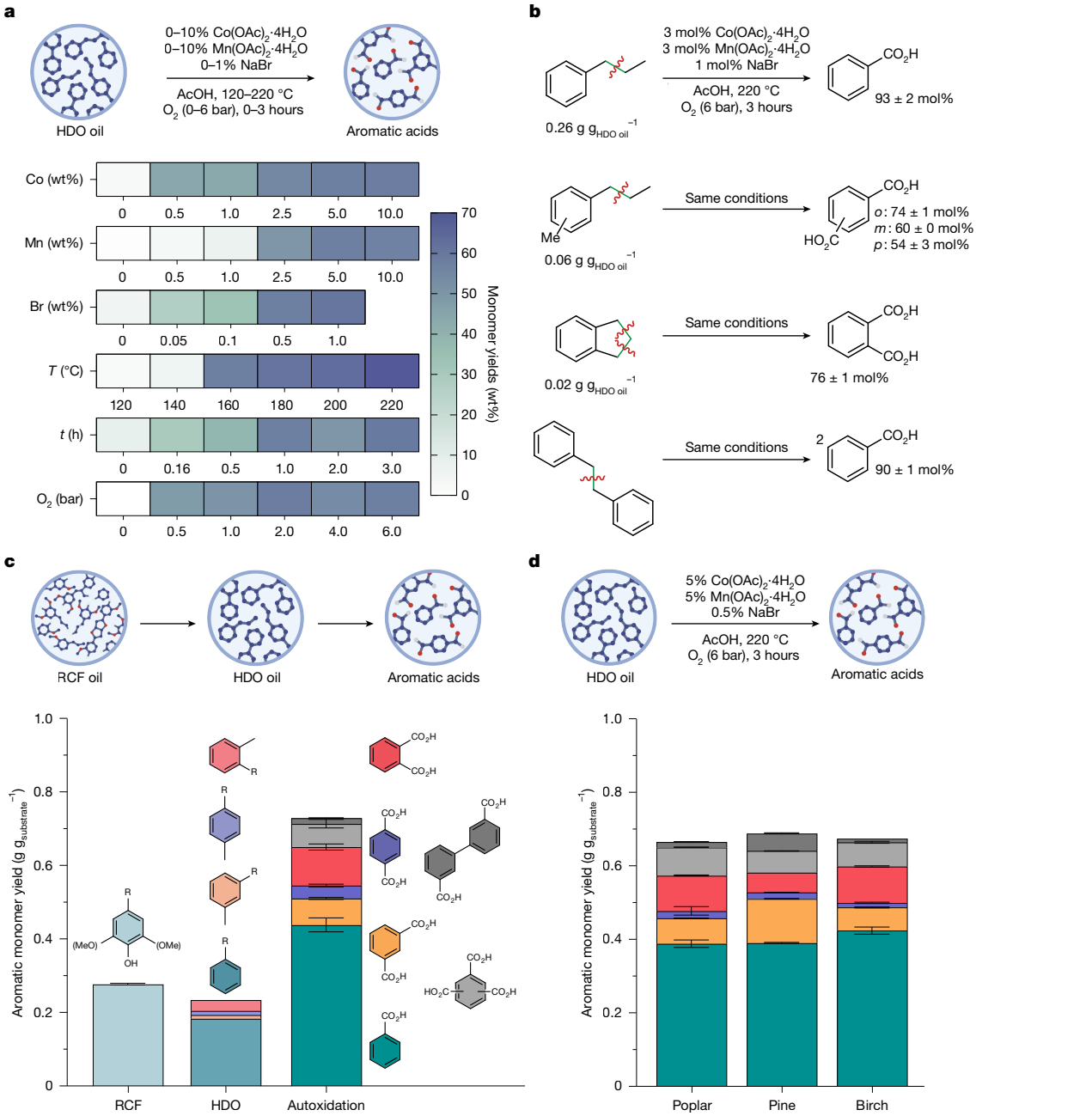

Fig. 2 | Catalytic autoxidation of lignin oil obtained via RCF and HDO. **a**, Top: reaction conditions for the optimization of the autoxidation reaction on poplar-derived HDO oil. Bottom: the effect of the reaction parameters on the autoxidation reaction. Monomer yields are defined as $\sum mass_{monomers\ in\ product}/mass_{HDO\ oil}$. **b**, Autoxidation of model compounds found in lignin HDO oil. Propylbenzene; *o*-, *m*- and *p*-methyl propylbenzene; indane and bibenzyl were used as model substrates. Relative abundances of model species in poplar-derived HDO oil are shown below the utilized substrate, with the exception of bibenzyl, which was not quantified owing to the large number of potential related isomers. Product yields are shown in mol%. Reported errors represent the range of duplicate experiments (half-range in either direction). **c**, Top: reaction scheme for HDO of poplar-derived RCF oil into HDO oil, followed by catalytic autoxidation of HDO oil to aromatic acids. Bottom: aromatic monomer yields of the RCF, HDO and autoxidation mixtures on a gram monomer per gram substrate basis (for RCF, g g^{-1} lignin; for HDO, g g^{-1} RCF oil; for autoxidation, g g^{-1} HDO oil). R groups of the most prevalent monomers are listed; distributions of individual monomers in RCF oil and HDO oil are shown in Suplementary Figs. 1 and 5, respectively. For RCF and autoxidation, the error bars show the mean half-range of duplicate and standard deviation of 27 runs, respectively. **d**, Comparison of autoxidation aromatic monomer yields (g g^{-1} HDO oil basis) across varying biomass feedstocks. The error bars show the range of duplicate experiments (half-range in either direction). MeOH, methanol; *t*, time; *T*, temperature; wt, weight; g, gram. Experimental details are in the Supplementary Materials. All data shown in this figure are available in Supplementary Data 1. Icons in panels **a**, **c** and **d** created in BioRender; Mains, K. https://BioRender.com/9hcf8sw (2026).

The three methyl-substituted propylbenzene isomers and indane are also effective substrates, converting all methyl and alkyl groups into aromatic carboxylic acids and forming the isomeric benzene dicarboxylic acid products in 54–76 mol% yield. Bibenzyl is converted into 2 equivalents of benzoic acid (90 mol% yield), demonstrating the conversion of a dimeric structure into monomers via oxidative C–C cleavage. Control reactions with benzoic acid, the three phthalic acids and the three benzene tricarboxylic acids (see below) at the same conditions result in substrate recoveries of 71–95 mol%, demonstrating product stability during the reaction (Supplementary Fig. 12). However,

biphenyl-3,3′-dicarboxylic acid (a product of 5–5′ interlinkages in lignin) showed more limited stability, with only a 49 mol% recovery observed under identical conditions. This lower yield of the dimeric product suggests that it may be degraded to either light gases or ring-opened products, as has been previously reported[8].

These promising results with well-defined small molecules set the stage for scaling the autoxidation of the HDO-derived lignin oil. The optimized conditions, when applied to the autoxidation of a 25 g l^{-1} solution of poplar-derived HDO oil, led to a mixture containing aromatic carboxylic acid monomers with a monomer yield of 73 ± 5 wt% ($Y_{mono} = \sum mass_{AO\ monomers}/mass_{HDO\ oil}$), equating to a monomer yield of 31 wt% on an initial lignin basis ($Y_{mono} = \sum mass_{AO\ monomers}/mass_{initial\ lignin}$). This outcome doubles the yield of aromatic carboxylic acids achieved under similar conditions from acetylated poplar RCF oil, as reported previously[7].

We finally investigated whether autoxidation was applicable to other biomass substrates by applying this chemistry to HDO-derived lignin oils from two additional woody substrates, pine and birch (Fig. 2d and Supplementary Fig. 14). Here we used our optimized conditions except for NaBr loading, which we reduced from 1 wt% to 0.5 wt%, owing to similar monomer yields resulting at both conditions in the aforementioned optimization study, combined with the desirability to operate at low catalyst loadings industrially. Monomer yields were nearly identical, fluctuating <2 wt% between poplar-, pine- and birch-derived HDO oils, at 67 ± 1 wt%, 69 ± 0.1 wt% and 67 ± 1 wt% (gram monomer per gram HDO oil basis), respectively. These results suggest feedstock flexibility for the process, at least among these three woody substrates. There appears to be an increase in fraction of *meta*-substituted monomers between the HDO oil and autoxidation substrate (that is, a larger fraction of isophthalate in the autoxidation substrate relative to *meta*-substituted alkyl aromatics in the feed) (Fig. 2c). Moreover, the highest isophthalate yield results from pine-derived substrate, suggesting that the increased isophthalate yield observed after autoxidation arises from the cleavage of β–5 bonds, which are more abundant in pine lignin relative to hardwood lignins and exhibit a *meta*-substituted functionality after deoxygenation[15,29] (Supplementary Fig. 6). These results highlight the ability of autoxidation to achieve high yields of aromatic monomers from multiple lignin-derived hydrocarbon feedstocks, substantially increasing the monomer quantities relative to those accessible from RCF alone.

Biological conversion to muconolactone

Separation of aromatic acids from the autoxidation stream is a challenge, and we thus sought to convert the mixed oxygenates to a single product through a biological funnelling approach[4,24,25]. Therefore, *P. putida* KT2440, which harbours aromatic catabolic pathways, is genetically tractable and shows tolerance to aromatic compounds[26,27], was engineered to convert the autoxidation products to a single molecule. As benzoate and the dicarboxylic acid isomers (that is, phthalates) comprise 93 mol% of the monomers present in the autoxidation-derived stream, we targeted a strain capable of converting these compounds to a convergent product, muconolactone. *P. putida* KT2440 natively uses benzoate via the catechol branch of the β-ketoadipate pathway[33] and has been engineered to catabolize terephthalate and isophthalate via the protocatechuate branch[34–37]. Although aerobic metabolism of phthalate to protocatechuate by *P. putida* NMH102 and *Comamonas* sp. E6 is known[38], this capability is not native in *P. putida* KT2440 (Supplementary Fig. 15), and heterologous expression of phthalate catabolism and transport genes from both microbes did not enable growth in *P. putida* KT2440 (Supplementary Fig. 16a). Catabolism of benzene tricarboxylic acids and biphenyl-3,3′-dicarboxylic acid is also not native to *P. putida* KT2440 (Supplementary Fig. 16b), and literature evidence of bacterial catabolism of these compounds is lacking; thus, discovery of these catabolic pathways is an opportunity for future investigation.

To engineer phthalate catabolism in *P. putida* KT2440, we enriched environmental samples for growth on phthalate, sequenced isolate genomes, and identified transporter and catabolic genes based on homology to known pathways in *P. putida* NMH102 and *Comamonas* sp. E6[38]. Environmental isolates AG8816 and AG8838 had near 100% 16S sequence identity to *Stutzerimonas stutzeri* KGS-2 and *Cupriavidus necator* N-1, respectively. Multiplexed serine-recombinase-assisted genome engineering[37,39] libraries were constructed using the bioprospected and reported[40,41] pathways, generating a pooled library of *P. putida* KT2440 strains containing different combinations of the transport and catabolic homologues (Supplementary Tables 1–4). Using growth-based selection, we found that the optimal combination for *P. putida* KT2440 growth on phthalate as a sole carbon and energy source was the OphP porin from *Comamonas* sp. E6, OphK transporter from AG8816, OphA1A2 dioxygenase from *Comamonas* sp. E6, OphB dehydrogenase from *Comamonas* sp. E6 and OphC decarboxylase from AG8816 (Supplementary Fig. 17).

We then genomically integrated these phthalate transport and catabolic genes with the isophthalate[37] and terephthalate[35] pathways into *P. putida* KT2440 via homologous recombination, generating strain AW521 (Fig. 3a, Supplementary Fig. 18 and Supplementary Tables 1–4). AW521 fully consumed benzoate and the three phthalate isomers in an equimolar mixture (10 mM total) within 24 h and grew on each as the sole carbon and energy sources at concentrations of 10 mM (Supplementary Figs. 15 and 19). Notably, growth was robust on all substrates except phthalate, which had a 24-h lag phase (Supplementary Figs. 15 and 19). The latter limitation was addressed by performing adaptive laboratory evolution[42] on 10-mM phthalate (Supplementary Fig. 20). Whole-genome sequencing of the growth-improved strains identified mutations including single nucleotide polymorphisms (SNPs) to the *ophK* ribosome binding site (Supplementary Fig. 21 and Supplementary Table 5). We reverse-engineered AW521 to include one of the identified SNPs and found that the mutation reduced the lag phase by 6-fold when grown on 10-mM phthalate while maintaining efficient growth on benzoate, isophthalate and terephthalate as the sole carbon and energy source (strain KMM026; Fig. 3b and Supplementary Figs. 22 and 23).

Finally, we sought to funnel the four main substrates (benzoate, isophthalate, terephthalate and phthalate) into muconolactone, which is produced non-enzymatically from (4,5-dihydro-5-oxofuran-2-yl)-acetate, the first common intermediate between the catechol and protocatechuate degradation pathways. We hypothesized that muconolactone could serve as a bioprivileged molecule[20] for the production of both adipic acid, a precursor to nylon 6,6, and dimethyl β-ketoadipic acid[43,44]. We targeted muconolactone instead of muconate, a commonly recognized bioproduct of interest[45–48], because of observed instability of muconic acid (that is, lower yields owing to a decrease in muconate titre over time in shake flasks) in initial biological conversion experiments using AW427, a *P. putida* KT2440 strain engineered to convert benzoate and terephthalate to muconate (Supplementary Fig. 24). Muconolactone requires half the base addition in bioreactor cultivations compared with muconate, which is an added benefit of this atom-efficient bioproduct.

Thus, we deleted *pcaD*, encoding the 3-oxoadipate enol-lactonase, from the phthalate-optimized strain (KMM026) to generate KMM037 (Fig. 3a and Supplementary Fig. 18) and compared performance on a poplar-derived autoxidation product mixture (autoxidation substrate) versus a mixture of commercially purchased compounds ('mock' mixture). The mock mixture contained relevant concentrations of all the identified aromatic compounds present in the autoxidation substrate, including benzene tricarboxylic acids and biphenyl-3,3′-dicarboxylic acid. The autoxidation substrate contained small amounts of acetate (1.3 ± 0.6 mM) owing to solvent carryover, which KMM037 utilized for growth along with a 20-mM glucose feed every 24 h. KMM037 fully utilized benzoate, phthalate, isophthalate and terephthalate within 24 h for both the mock mixture and autoxidation substrate, achieving

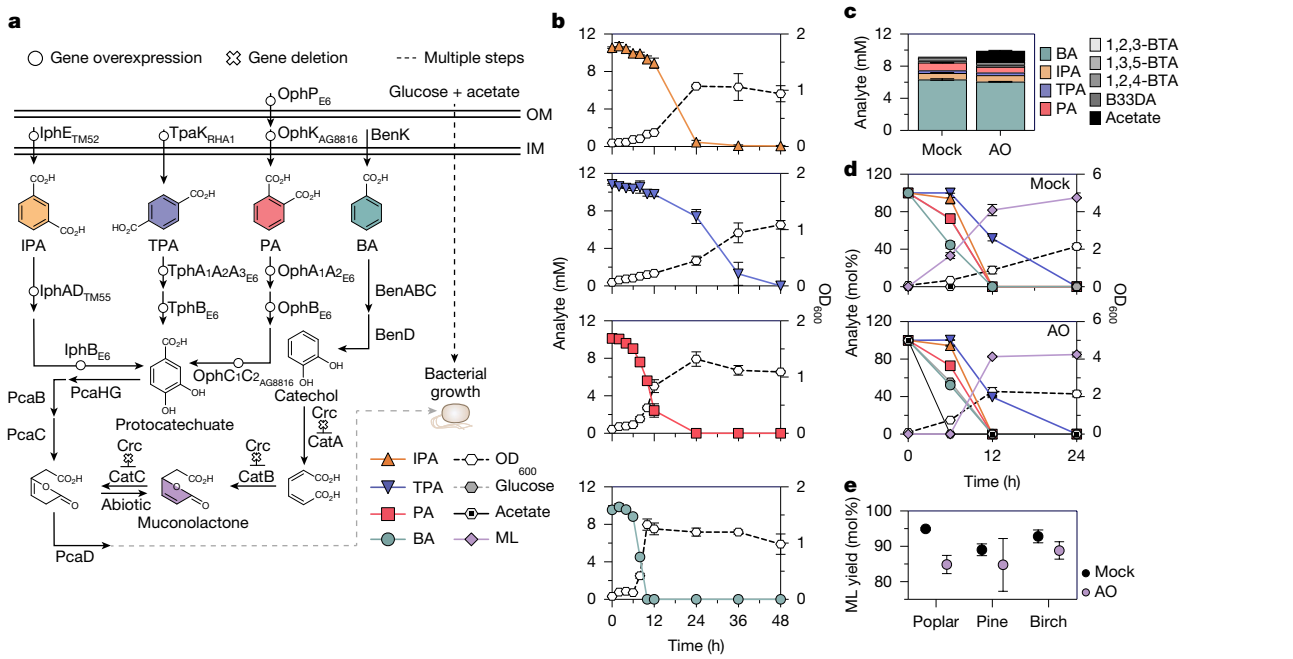

Fig. 3 | Bioconversion of autoxidation-derived aromatic compound mixtures to muconolactone. a, Schematic of engineered catabolic pathways for isophthalate (IPA), terephthalate (TPA) and phthalate (PA) alongside the native benzoate (BA) pathway in *P. putida* KT2440. Pathway integration enables growth (strain KMM026) or, with *pcaD* deletion, muconolactone production (strain KMM037) from the primary monomers from autoxidation. All aromatic pathway intermediates and enzyme abbreviations are detailed in Supplementary Fig. 18. Subscripts indicate a protein of heterologous origin. OM and IM indicate the outer membrane and inner membrane, respectively. Genotypes and strain construction details are provided in Supplementary Tables 1–4. **b**, All four primary aromatic monomers from autoxidation are consumed by KMM026 as the sole carbon and energy source in shake-flask cultivations. **c**, Molar composition of aromatic substrates used in the mock mixture (commercial compounds) and the autoxidation (AO) substrate (derived from poplar as described above; Fig. 2c). In addition to quantified aromatic analytes, the autoxidation substrate contains unquantified unknowns. **d**, KMM037 shake-flask cultivations with 20-mM glucose and either (top) 10 mM of mock mixture or (bottom) 10-mM poplar-derived autoxidation (AO) substrate (Fig. 2c) showing conversion of all provided benzoate, phthalate, terephthalate and isophthalate to muconolactone (ML) within 24 h. Extended time profiles with molar substrate concentrations are provided in Supplementary Fig. 25. **e**, Muconolactone (ML) yields measured at 24 h for KMM037 shake-flask cultivations with 20-mM glucose and either 10 mM of mock mixture or 10-mM autoxidation substrate derived from poplar (Figs. 2c and 3d), pine or birch (Fig. 2d). Time-course profiles with molar substrate concentrations for pine- and birch-derived substrates are provided in Supplementary Fig. 26. For panels **b**–**e**, the data show the average of three biological replicates and error bars depict the standard deviation. BTA, benzene tricarboxylic acid; B33DA, biphenyl-3, 3′-dicarboxylic acid; OD_{600}, optical density, measured as absorbance at 600 nm. All data shown in this figure are available in Supplementary Data 1. Bacterial growth icon in panel **a** adapted with permission from ref. 36, AAAS.

muconolactone molar yields of 95 ± 0.3% and 85 ± 2%, respectively ($Y_{muconolactone}$ = $mol_{muconolactone\ produced}/\sum mol_{bioavailable\ aromatics\ fed}$; Fig. 3c,d and Supplementary Fig. 25). Here, and throughout the text, we define bioavailable aromatics as the sum of benzoate, terephthalate, isophthalate and phthalate. Full conversion of the aromatic substrates at <100% muconolactone yields suggests build-up of unquantified metabolic intermediates (standards are not available); no build-up of protocatechuate or catechol was observed. In addition, KMM037 successfully converted benzoate, phthalate, isophthalate and terephthalate derived from pine and birch (Fig. 2d) to muconolactone at molar yields of 85 ± 7% and 89 ± 2%, respectively (Fig. 3e and Supplementary Fig. 26). Muconolactone yields from pine- and birch-derived substrates compared with relevant mock mixtures did not differ significantly (two-tailed *P* value >0.05). Across all the autoxidation substrates fed to KMM037 in shake flasks, muconolactone yields fluctuated <5 mol%, suggesting the biological conversion of aromatic monomers to muconolactone is promising for the three woody biomass feedstocks tested.

Bioconversion scale-up

The cultivations were scaled to 0.5-l bioreactors to evaluate titres, yields and productivities in process-relevant conditions. To optimize the bioprocess, we first used mock mixtures of the autoxidation substrate, which contained relevant concentrations of all the aromatics present including benzene tricarboxylic acids and biphenyl-3,3′-dicarboxylic acid. First, bioreactor cultivations were conducted in dissolved oxygen (DO)-stat-fed-batch mode, which showed that a 1:1 aromatics-to-glucose ratio was optimal in the feed (Supplementary Figs. 27 and 28). Next, the production in a DO-stat controlled cultivation was compared with a constant rate fed-batch process controlled at 4 mM, 6 mM, and 12 mM bioavailable aromatic compounds per hour feeding rates (relative to the initial batch volume) to increase productivity compared with the DO-stat-fed-batch-controlled cultivations (Supplementary Figs. 29–33). Feeding at a constant rate of 6 mM h^{-1} resulted in the highest maximum muconolactone titre of 25 ± 1 g l^{-1} with a yield of 89 ± 3 mol%, selectivity of 104 ± 1 mol% and productivity of 0.35 ± 0.01 g l^{-1} h^{-1} (where yield is $Y_{muconolactone}$ = $mol_{muconolactone\ produced}/\sum mol_{bioavailable\ aromatics\ fed}$ and selectivity is $S_{muconolactone}$ = $mol_{muconolactone\ produced}/\sum mol_{bioavailable\ aromatics\ consumed}$; Fig. 4a and Supplementary Fig. 31). Lastly, we produced muconolactone from the poplar-derived autoxidation substrate (Fig. 2c) in bioreactors operated in DO-stat-fed-batch mode and in constant rate fed-batch mode with a feed rate of 6 mM h^{-1} (Fig. 4b and Supplementary Figs. 34–36). The strain produced 9 g l^{-1} and 18 g l^{-1} muconolactone at yields of 84 mol% and 78 mol%, and selectivities of 87 mol% and 83 mol% in DO-stat-fed and constant-fed-batch (6 mM h^{-1}) modes, respectively.

Comparing strain performance in bioreactors with mock and autoxidation substrate conducted in fed-batch mode with a constant feed rate, we observe lower maximum titres (18 g l^{-1} versus 25 g l^{-1}), selectivity (100 mol% versus 83 mol%) and yield (89 mol% versus 78 mol%), calculated at those maximum titres, for the autoxidation substrate and

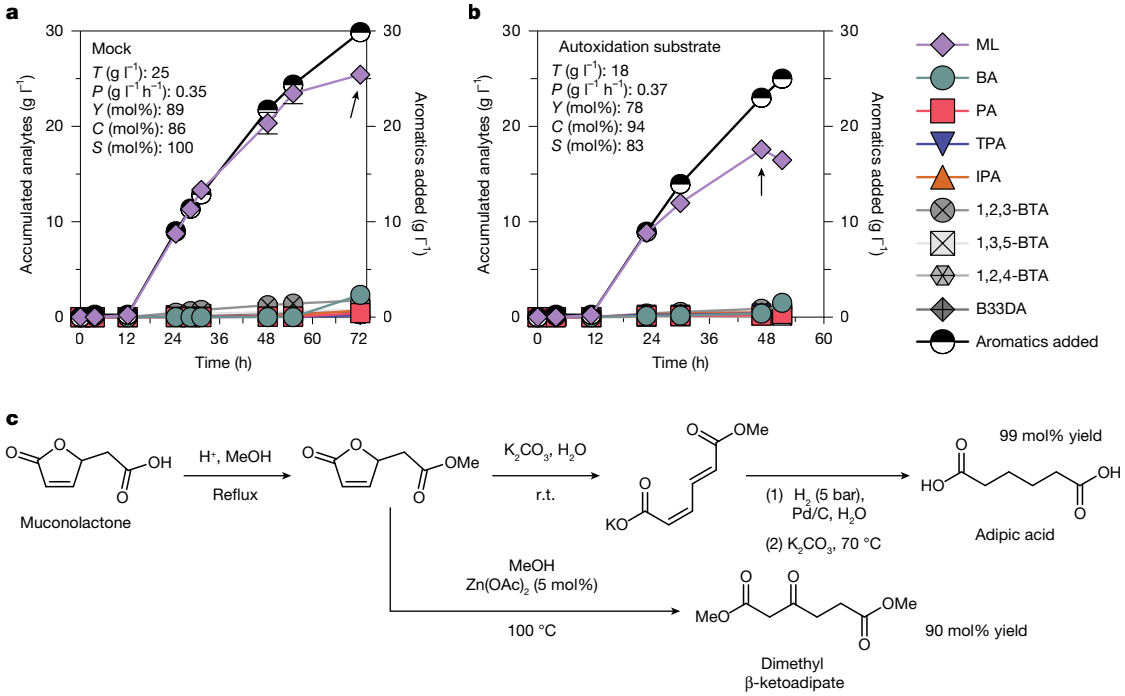

Fig. 4 | Scale up of muconolactone production and conversion to adipic acid. a,**b**, KMM037 cultivated in fed-batch bioreactors with a constant 6 mM h^{-1} feed rate of a mock aromatic substrate (**a**) and the autoxidation substrate (**b**), both in an equimolar mix with glucose (1:1 molar ratio of aromatics:glucose). The mock aromatic substrate consisted of commercial compounds at concentrations equivalent to that of autoxidation substrate. Aromatics and muconolactone accumulated (left *y* axis) and aromatics fed (right *y* axis) are plotted as a function of time. The arrows indicate the time point at which maximum titre (*T*), rate (*R*), yield (*Y*), conversion (*C*) and selectivity (*S*) are reported in the top-left corner. Here yield is $Y_{muconolactone} = mol_{muconolactone\ produced}/\sum mol_{bioavailable\ aromatics\ fed}$, conversion is $C = \sum mol_{bioavailable\ aromatics\ consumed}/\sum mol_{bioavailable\ aromatics\ fed}$, and selectivity is $S_{muconolactone} = mol_{muconolactone\ produced}/\sum mol_{bioavailable\ aromatics\ consumed}$. Bioavailable aromatics represent the sum of benzoate, terephthalate, isophthalate and phthalate. Bioreactor cultivations with the mock aromatic substrate were performed in duplicate; error bars depict the absolute error between replicates. The bioreactor cultivation on the autoxidation substrate was done in singlet because of substrate limitations. Numerical data are provided in Supplementary Data 1; growth profiles are provided in Supplementary Figs. 31 and 35 for **a** and **b**, respectively. **c**, Chemical conversion of muconolactone to adipic acid and dimethyl β-ketoadipate. ^{1}H NMR spectroscopy yields for the conversion of muconolactone to adipic acid and dimethyl β-ketoadipate are 99 mol% and 90 mol%, respectively. Me, methyl. All data shown in this figure are available in Supplementary Data 1.

the mock media, respectively (Fig. 4a,b and Supplementary Fig. 37). Conversion (*C*) of substrate (where $C = \sum mol_{bioavailable\ aromatics\ consumed}/\sum mol_{bioavailable\ aromatics\ fed}$), however, remains high at 94 mol% when the maximum titre was achieved for the autoxidation substrate case. Similar to the shake-flask cultivations, the reduced selectivity and yield points towards the build-up of unquantified metabolic intermediates (standards are not available). Notably, cells reached the death phase earlier when fed the autoxidation substrate, 51 h compared with 72 h. We hypothesized that the difference in strain performance is caused by either (1) remaining catalyst components (metals or acetic acid) or (2) unquantified toxic side products in the autoxidation substrate. Catalyst components (Mn, Co and Br) were below the limit of quantification in the autoxidation substrate prepared for biological cultivations (Supplementary Table 6); sodium was present but at too low a concentration (6 mM) to impact strain performance[49]. In addition, no acetate build-up was observed over the course of the culture, suggesting that any acetate present in the autoxidation substrate was utilized for cell growth. To determine whether unquantified toxic side products are the cause of early cell death, we chose a class of known side products resulting during autoxidation—alkyl benzoic acids[22]—and fed a representative compound from this class, *o*-toluic acid, to KMM037 alongside glucose at increasing concentrations. While the plasmid-containing parent strain of *P. putida* KT2440, *P. putida* mt-2, is known to metabolize toluic acid and xylene, *P. putida* KT2440 cannot metabolize alkylated benzenes[50]. We tested *o*-toluic acid concentrations up to 100 mM and observed toxicity effects (for example, increased lag phase and reduced growth rate) at 50 mM (7 g l^{-1}) and above (Supplementary Fig. 38). Thus, we infer that the accumulation of aromatic intermediates present in the autoxidation substrate may limit bioconversion.

Synthesis of nylon monomers

We next sought to convert muconolactone to adipic acid, a monomer for nylon 6,6, and dimethyl β-ketoadipic acid, a monomer for performance-advantaged nylons[43,44]. Muconolactone has been identified as the product of acid catalysed ring-closure of *cis*,*trans*-muconic acid[51], and as an intermediate in the production of levulinic acid from muconic acid[52]. Muconic acid is a well-documented bio-based platform molecule[48], with the most common application being hydrogenation to adipic acid[45–47]. Hence, we first targeted muconolactone conversion to adipic acid via muconic acid (Fig. 4c). We found that by protecting the acid group on muconolactone with a methyl ester (Supplementary Fig. 39), the lactone readily ring-opened from the γ-position using 1 equivalent of K_2CO_3 in water at room temperature. The reaction selectively formed the *cis*,*trans*-methyl potassium muconate salt in quantitative yield by ^{1}H NMR spectroscopy (Supplementary Fig. 40). The aqueous mixture was hydrogenated to potassium methyl adipate using Pd/C (5 wt%, 5 bar H_2, 25 °C) (Supplementary Fig. 41). At this stage, another equivalent of K_2CO_3 was added and heated to 70 °C to hydrolyse the methyl ester. After acidification, adipic acid production was confirmed by ^{1}H NMR spectroscopy at 99 mol% yield, with an unoptimized 88% isolated yield (Supplementary Fig. 42). Alternatively, muconolactone methyl ester was ring-opened with methanol, catalysed by a primary alcohol using a Lewis acid catalyst, such as $Zn(OAc)_2$ (10 mol%) at

100 °C, to give dimethyl β-ketoadipate in 90 mol% yield by ^{1}H NMR spectroscopy (Fig. 4c and Supplementary Figs. 43 and 44). In its free acid form, β-ketoadipic acid readily decarboxylates, limiting its practical use. With this method, via muconolactone methyl ester, stable molecules can be accessed that could be used in performance-advantaged polymers and polymer additives[43,44].

Conclusion

Taken together, this work demonstrates a proof-of-concept process for lignin conversion to single products (for example, adipic acid). Although the HDO, autoxidation and biological funnelling steps feature unavoidable losses that impact the total carbon yield—for example, through formation of methane and carbon dioxide—the process can generate a theoretical yield of 57 wt% (gram product per gram lignin basis) (Fig. 1b and Extended Data Figs. 1 and 2). In practice, with unoptimized small-scale processes and inherent transfer losses, this sequence achieved up to 26 wt% yield of adipic acid relative to the lignin in the original biomass (0.26 g adipic acid per gram lignin). The two-step HDO-oxidation approach on extracted lignin allows for initial removal of inhibitory phenolic groups, thus enabling facile C–C bond cleavage of oligomeric aromatic hydrocarbons, well beyond the C–O bond cleavage limit that confine nearly all selective lignin depolymerization technologies[5]. Furthermore, the high monomer content and water solubility (100 g l^{-1}) of the produced autoxidation product enhances downstream bioconversion compared with other lignin deconstruction methods (for example, RCF). The HDO and oxidation steps both utilize industrial chemistries and thus could leverage existing manufacturing infrastructure. We acknowledge that starting with RCF to generate a low-molar-mass product initially is a limitation of this method, as the process currently has techno-economic constraints that need to be solved to enable a viable process[53,54]. However, analogous processes have the potential to be applied towards condensed lignin substrates (for example, Kraft lignin), pending future development. With further metabolic engineering, the present bioconversion approach can be expanded and tuned to include increasingly complex autoxidation products (for example, benzene tricarboxylic acids) and target virtually any biologically accessible product[55].

Online content

Any methods, additional references, Nature Portfolio reporting summaries, source data, extended data, supplementary information, acknowledgements, peer review information; details of author contributions and competing interests; and statements of data and code availability are available at https://doi.org/10.1038/s41586-026-10580-x.

1. Liao, Y. et al. A sustainable wood biorefinery for low-carbon footprint chemicals production. *Science* **367**, 1385–1390 (2020).
2. Meng, Q. et al. Sustainable production of benzene from lignin. *Nat. Commun.* **12**, 4534 (2021).
3. Subbotina, E. et al. Oxidative cleavage of C–C bonds in lignin. *Nat. Chem.* **13**, 1118–1125 (2021).
4. Werner, A. Z. et al. Lignin conversion to β-ketoadipic acid by *Pseudomonas putida* via metabolic engineering and bioprocess development. *Sci. Adv.* **9**, eadj0053 (2023).
5. Schutyser, W. et al. Chemicals from lignin: an interplay of lignocellulose fractionation, depolymerisation, and upgrading. *Chem. Soc. Rev.* **47**, 852–908 (2018).
6. Questell-Santiago, Y. M., Galkin, M. V., Barta, K. & Luterbacher, J. S. Stabilization strategies in biomass depolymerization using chemical functionalization. *Nat. Rev. Chem.* **4**, 311–330 (2020).
7. Gu, N. X. et al. Autoxidation catalysis for carbon–carbon bond cleavage in lignin. *ACS Cent. Sci.* **9**, 2277–2285 (2023).
8. Palumbo, C. T. et al. Catalytic carbon–carbon bond cleavage in lignin via manganese–zirconium-mediated autoxidation. *Nat. Commun.* **15**, 862 (2024).
9. Palumbo, C. T. et al. Accessing monomers from lignin through carbon–carbon bond cleavage. *Nat. Rev. Chem.* **8**, 799–816 (2024).
10. Tomás, R. A. F., Bordado, J. C. M. & Gomes, J. F. P. *p*-Xylene oxidation to terephthalic acid: a literature review oriented toward process optimization and development. *Chem. Rev.* **113**, 7421–7469 (2013).
11. Speight, J. Petroleum refinery processes. In *Kirk-Othmer Encyclopedia of Chemical Technology* (Wiley, 2018); https://doi.org/10.1002/0471238961.1805060919160509.a01.pub3.
12. Musser, M. T. Cyclohexanol and cyclohexanone. In *Ullmann's Encyclopedia of Industrial Chemistry* (Wiley, 2000); https://doi.org/10.1002/14356007.a08_217
13. Zakzeski, J., Bruijnincx, P. C. A., Jongerius, A. L. & Weckhuysen, B. M. The catalytic valorization of lignin for the production of renewable chemicals. *Chem. Rev.* **110**, 3552–3599 (2010).
14. Sun, Z., Fridrich, B., de Santi, A., Elangovan, S. & Barta, K. Bright side of lignin depolymerization: toward new platform chemicals. *Chem. Rev.* **118**, 614–678 (2018).
15. Ralph, J., Lapierre, C. & Boerjan, W. Lignin structure and its engineering. *Curr. Opin. Biotechnol.* **56**, 240–249 (2019).
16. Lucarini, M. & Pedulli, G. F. Free radical intermediates in the inhibition of the autoxidation reaction. *Chem. Soc. Rev.* **39**, 2106–2119 (2010).
17. Stone, M. L. et al. Continuous hydrodeoxygenation of lignin to jet-range aromatic hydrocarbons. *Joule* **6**, 2324–2337 (2022).
18. Webber, M. S. et al. Lignin deoxygenation for the production of sustainable aviation fuel blendstocks. *Nat. Mater.* **23**, 1622–1638 (2024).
19. Webber, M. S. et al. Drop-in sustainable aviation fuels enabled by feedstock-agnostic lignin deoxygenation. *Cell Rep. Phys. Sci.* **6**, 102687 (2025).
20. Shanks, B. H. & Keeling, P. L. Bioprivileged molecules: creating value from biomass. *Green Chem.* **19**, 3177–3185 (2017).
21. Cywar, R. M., Rorrer, N. A., Hoyt, C. B., Beckham, G. T. & Chen, E. Y. X. Bio-based polymers with performance-advantaged properties. *Nat. Rev. Mater.* **7**, 83–103 (2021).
22. Partenheimer, W. Methodology and scope of metal/bromide autoxidation of hydrocarbons. *Catal. Today* **23**, 69–158 (1995).
23. Partenheimer, W. The aerobic oxidative cleavage of lignin to produce hydroxyaromatic benzaldehydes and carboxylic acids via metal/bromide catalysts in acetic acid/water mixtures. *Adv. Synth. Catal.* **351**, 456–466 (2009).
24. Liu, A. et al. Biomanufacturing of value-added chemicals from lignin. *Curr. Opin. Biotechnol.* **89**, 103178 (2024).
25. Pereyra-Camacho, M. A. & Pardo, I. Biological degradation of phthalates: from bioremediation to plastic waste valorization. *ChemSusChem* **19**, e202501955 (2026).
26. Weimer, A., Kohlstedt, M., Volke, D. C., Nikel, P. I. & Wittmann, C. Industrial biotechnology of *Pseudomonas putida*: advances and prospects. *Appl. Microbiol. Biotechnol.* **104**, 7745–7766 (2020).
27. Martínez-García, E. & de Lorenzo, V. *Pseudomonas putida* as a synthetic biology chassis and a metabolic engineering platform. *Curr. Opin. Biotechnol.* **85**, 103025 (2024).
28. Abu-Omar, M. M. et al. Guidelines for performing lignin-first biorefining. *Energy Environ. Sci.* **14**, 262–292 (2021).
29. Dao Thi, H. et al. Identification and quantification of lignin monomers and oligomers from reductive catalytic fractionation of pine wood with GC × GC – FID/MS. *Green Chem.* **24**, 191–206 (2022).
30. Sullivan, M. M., Chen, C.-J. & Bhan, A. Catalytic deoxygenation on transition metal carbide catalysts. *Catal. Sci. Technol.* **6**, 602–616 (2016).
31. Gong, W. H. In *Industrial Arene Chemistry* (ed. Mortier, J.) 1107–1135 (Wiley, 2023).
32. Weeda, E. P. et al. O_2-permeable membrane reactor for continuous oxidative depolymerization of lignin. *Joule* **8**, 3336–3346 (2024).
33. Jiménez, J. I., Miñambres, B., García, J. L. & Díaz, E. Genomic analysis of the aromatic catabolic pathways from *Pseudomonas putida* KT2440. *Environ. Microbiol.* **4**, 824–841 (2002).
34. Fuchs, G., Boll, M. & Heider, J. Microbial degradation of aromatic compounds—from one strategy to four. *Nat. Rev. Microbiol.* **9**, 803–816 (2011).
35. Werner, A. Z. et al. Tandem chemical deconstruction and biological upcycling of poly(ethylene terephthalate) to β-ketoadipic acid by *Pseudomonas putida* KT2440. *Metab. Eng.* **67**, 250–261 (2021).
36. Sullivan, K. P. et al. Mixed plastics waste valorization through tandem chemical oxidation and biological funneling. *Science* **378**, 207–211 (2022).
37. Huenemann, J. D. et al. Combinatorial pathway engineering using multiplex serine recombinase-assisted genome engineering (mSAGE). Preprint at *bioRxiv* https://doi.org/10.1101/2025.07.11.664204 (2025).
38. Boll, M., Geiger, R., Junghare, M. & Schink, B. Microbial degradation of phthalates: biochemistry and environmental implications. *Environ. Microbiol. Rep.* **12**, 3–15 (2019).
39. Elmore, J. R. et al. High-throughput genetic engineering of nonmodel and undomesticated bacteria via iterative site-specific genome integration. *Sci. Adv.* **9**, eade1285 (2023).
40. Nomura, Y., Harashima, S. & Oshima, Y. PHT, a transmissible plasmid responsible for phthalate utilization in *Pseudomonas putida*. *J. Ferment. Bioeng.* **70**, 295–300 (1990).
41. Shimodaira, J. et al. Draft genome sequence of *Comamonas* sp. strain E6 (NBRC 107749), a degrader of phthalate isomers through the protocatechuate 4,5-cleavage pathway. *Genome Announc.* **3**, e0064315 (2015).
42. Sandberg, T. E., Salazar, M. J., Weng, L. L., Palsson, B. O. & Feist, A. M. The emergence of adaptive laboratory evolution as an efficient tool for biological discovery and industrial biotechnology. *Metab. Eng.* **56**, 1–16 (2019).
43. Johnson, C. W. et al. Innovative chemicals and materials from bacterial aromatic catabolic pathways. *Joule* **3**, 1523–1537 (2019).
44. Rorrer, N. A. et al. Production of β-ketoadipic acid from glucose in *Pseudomonas putida* KT2440 for use in performance-advantaged nylons. *Cell Rep. Phys. Sci.* **3**, 100840 (2022).
45. Vardon, D. R. et al. *cis*,*cis*-Muconic acid: separation and catalysis to bio-adipic acid for nylon-6,6 polymerization. *Green Chem.* **18**, 3397–3413 (2016).
46. Capelli, S. et al. Bio-adipic acid production by catalysed hydrogenation of muconic acid in mild operating conditions. *Appl. Catal. B* **218**, 220–229 (2017).
47. Capelli, S. et al. Bio adipic acid production from sodium muconate and muconic acid: a comparison of two systems. *ChemCatChem* **11**, 3075–3084 (2019).

48. Khalil, I., Quintens, G., Junkers, T. & Dusselier, M. Muconic acid isomers as platform chemicals and monomers in the biobased economy. *Green Chem.* **22**, 1517–1541 (2020).
49. Wilkes, R. A. et al. Comparison of microbial strains as candidate hosts and genetic reservoirs for the valorization of lignin streams. *Green Chem.* **26**, 12053–12069 (2024).
50. Worsey, M. J. & Williams, P. A. Metabolism of toluene and xylenes by *Pseudomonas* (*putida* (*arvilla*) mt-2: evidence for a new function of the TOL plasmid. *J. Bacteriol.* **124**, 7–13 (1975).
51. Carraher, J. M., Pfennig, T., Rao, R. G., Shanks, B. H. & Tessonnier, J.-P. *cis*,*cis*-Muconic acid isomerization and catalytic conversion to biobased cyclic-C_6-1,4-diacid monomers. *Green Chem.* **19**, 3042–3050 (2017).
52. Ver Elst, C. et al. Synthesis of levulinic acids from muconic acids in hot water. *Angew. Chem. Int. Ed.* **62**, e202309597 (2023).
53. Bartling, A. W. et al. Techno-economic analysis and life cycle assessment of a biorefinery utilizing reductive catalytic fractionation. *Energy Environ. Sci.* **14**, 4147–4168 (2021).
54. Arts, W. et al. Stepping away from purified solvents in reductive catalytic fractionation: a step forward towards a disruptive wood biorefinery process. *Energy Environ. Sci.* **16**, 2518–2539 (2023).
55. Lee, S. Y. et al. A comprehensive metabolic map for production of bio-based chemicals. *Nat. Catal.* **2**, 18–33 (2019).

Methods

Chemicals

Unless otherwise stated, all reagents were purchased from commercial sources and used without further purification. A list of the chemicals used in this study can be found in Supplementary Information.

Large-scale RCF

The following procedure was performed with poplar (ten runs; Fig. 2c and Supplementary Figs. 1–4). Under a flow of nitrogen, 300 g poplar biomass and 30 g 5% Ru/C were added to a 7.5-l Parr batch reactor vessel. Next, 1 l water was added followed by 2 l methanol. The vessel was pressure tested with nitrogen (117 bar), where the maximum acceptable loss was 7 mbar min^{-1}. Subsequently, the reactor was flushed twice with 27.6 bar of nitrogen to sparge the vessel of any residual air. Once all the nitrogen was drained, the vessel was pressured with hydrogen (30 bar). The mixture was then heated (225 °C) with the mag drive set to 80% of maximum stirring, and cooling water was run through the mag drive. After 3 h, the vessel was rapidly cooled with water through a cooling coil. The vessel was depressurized, and the product was pumped out of the mixture using a peristaltic pump. The methanol was removed by rotary evaporation, and the residual was extracted with equivolume dichloromethane. The water fraction was extracted two more times with dichloromethane, the organic layers were combined, washed again with water and dried with sodium sulfate, and dichloromethane was evaporated by rotary evaporation. A total yield of 280.7 g of lignin oil was obtained. For reactions accurately measuring oil yield, the above procedure was done identically, with the only difference being that the pulp was taken from the reactor after pumping out the reaction liquor and vigorously washed with 6 l methanol before rotary evaporation.

Small-scale RCF

Small-scale RCF of poplar biomass was conducted in 75-ml Parr autoclave reactors with a Parr 5000 Multiple Reactor System (Supplementary Fig. 2). Before reaction, 3 g biomass, 300 mg 5 wt% Ru/C, 20 ml methanol, and 10 ml water were loaded into the reactor and the system was sealed. The reactor was subsequently pressure tested at 60 bar with nitrogen and then flushed twice with 30 bar nitrogen. The system was then pressurized to 30 bar with hydrogen and stirring was set to 700 rpm with a Teflon stir bar. The sealed system was heated to 225 °C over 30 min and held for 3 h. The reactors were then immediately quenched in ice water to room temperature and depressurized. The reactor contents were then passed through a polytetrafluoroethylene frit filter (Chemglass, 10 μm), and the residual solids were vigorously washed with 200–300 ml methanol. The resulting reaction liquor was then dried via rotary evaporation, and liquid–liquid extracted with 10 ml/10 ml of water/dichloromethane. The aqueous phase was washed twice more with 5 ml dichloromethane. The organic phases were combined and rotary evaporated to dryness before massing and characterization, resulting in an oil yield of 74 wt% for duplicate reactions.

Trickle-bed reactor design and dimensions for HDO

Deoxygenation reactions were performed in a trickle-bed reactor using a similar design to that reported previously[17,19]. The reactor consisted of a 21″ long, 1/2″ OD Hastelloy reactor tube located in a vertically mounted, insulated, single-zone, split furnace (Applied Test Systems Series 3210) with steel heat transfer blocks to fill void space. Two K-type thermocouples were used for temperature regulation. One thermocouple, contacting the outside of the steel heat transfer blocks, was used for temperature control along with a Digi-sense TC9600 PID controller. Meanwhile, the other was slotted to contact the outside of the reactor tube in the centre of the heating zone and used to probe reaction temperature. Liquid was fed using a Teledyne ISCO 1000D Syringe Pump, which fed into a 1/8″ OD 316 stainless steel drip tube leading to the heated reaction zone at the top of the reactor. Gas flow rates were controlled using mass flow controllers (Brooks SLA5850S-1BAB1C2A1), which fed into the top of the reactor co-currently with the liquid via 1/2″ 316 stainless steel tubing. Gas/liquid separation was done at room temperature using a Jerguson glass level gauge. Downstream of the gauge, a diaphragm back-pressure regulator (Equilibar H3P1SNN8-NSBP1500T100G20KK) was used to maintain system pressure. A separate nitrogen back-fill line was used to maintain constant system pressure during liquid sampling via a needle valve (Swagelok).

The reactors were packed as follows before catalyst pre-treatment: a quartz wool (Technical Glass Products) plug was placed in the bottom of the reactor tube, followed by 9.75″ of quartz chips (fused (granular), Sigma-Aldrich, sieved 10–20 mesh), another quartz wool plug, the catalyst bed, another quartz wool plug, and finally more quartz chips up to 1″ below the level of the drip tube. The plugs and quartz packing minimized the reactor hold-up volume while helping to secure the position of the catalyst bed.

HDO catalyst synthesis

Catalyst synthesis was conducted as previously reported[17,19]. In brief, ammonium molybdate tetrahydrate (ACS reagent grade, Fisher Scientific) was sieved between 60 and 100 mesh. Next, 15 g ammonium molybdate tetrahydrate was loaded into the reactor to generate 8.6 g Mo_2C. A heating ramp from 25 °C to 680 °C was done over 3.5 h, then held for another 3.5 h under 165 ml min^{-1} hydrogen (UHP, Airgas) and 45 ml min^{-1} of methane (UHP, Airgas). Methane flow was then stopped and a subsequent 30-min scavenging step was conducted under pure hydrogen gas to clear the catalyst surface of polymeric carbon. The reactor was then cooled to room temperature under hydrogen flow before the reaction start.

Feed preparation for HDO

Neat lignin oil was used after generation via RCF using the procedure outlined above. Ten batches of oil were combined, resulting in 270 g feed in total after transfer losses. Partially deoxygenated lignin oil used for the second reaction pass was prepared as described previously[17,19]. Steady-state first-pass reaction samples were combined after removing enough sample for analysis. The water fraction was allowed to phase-separate from the combined sample and removed via pipette, with the organic phase then being used directly without treatment.

Running trickle-bed reactions for HDO

Reactions were run as described previously[17,19]. After catalyst synthesis, the reactor was cooled to room temperature under flowing hydrogen. The reactor was then pressurized via nitrogen back-fill to 900 psi and hydrogen flow was adjusted to the desired rate for reaction (270 ml min^{-1}). The reactor was heated to the desired reaction temperature (350 °C and 375 °C for first pass and second pass, respectively) under flowing toluene at 3 ml min^{-1} to pre-wet the catalyst bed. When the reactor approached 300 °C, near the critical temperature of toluene (320 °C), the liquid feed was switched to neat lignin oil at 0.3 ml min^{-1}. Samples were subsequently taken every 30 min for the duration of the reaction from the needle valve as described above. HDO-derived lignin oils from pine and birch were sourced from previously published work[19], where detailed procedures and analyses are reported.

General procedure for autoxidation reaction of the HDO lignin oil and model compounds

For a single optimization reaction, a 75-ml Parr grade 4 corrosion resistant titanium batch reactor fit with a glass liner insert was charged with 50–1,000 mg of HDO oil, acetic acid (20 ml), a stir bar, and catalyst components $Co(OAc)_2{\cdot}4H_2O$, $Mn(OAc)_2{\cdot}4H_2O$ and NaBr (0–10 wt%, 0–10 wt% and 0–2 wt%, respectively). The mixture was purged 3 times with an inert gas (N_2; 30 bar) and subsequently charged with zero air to achieve the desired partial oxygen pressure (1 bar oxygen ≈ 5 bar zero air), with the balance being charged with nitrogen to achieve a

total reactor pressure of 60 bar in all cases. The vessel was heated to 120–220 °C (heat-up time about 30 min), at which temperature it was held for 0–180 min before it was cooled rapidly in an ice bath. The solutions were frozen until needed for analysis.

Isolation of the autoxidation mixture for biological conversion

Under the optimized conditions, a 75-ml Parr grade 4 corrosion resistant titanium batch reactor fitted with a glass liner insert was charged with 500 mg HDO oil, acetic acid (20 ml), a stir bar, and catalyst components $Co(OAc)_2{\cdot}4H_2O$, $Mn(OAc)_2{\cdot}4H_2O$ and NaBr (5 wt%, 5 wt% and 1 wt%, respectively). The mixture was pressurized 3 times with an inert gas (N_2) and subsequently charged with zero air to achieve 6 bar partial pressure of oxygen. The vessel was heated to 220 °C (heat-up time about 30 min), at which temperature it was held for 3 h before it was cooled rapidly in an ice bath. The reaction was carried out 27 times (Supplementary Table 7). The solutions were frozen until needed for analysis. Once all the reactions were complete, all the solutions of products obtained from the 27 runs were mixed. Liquid–liquid extraction (0.1% HCl aq./Et_2O) of the obtained mixture was repeatedly performed to separate the catalysts from the products. For each extraction, a ratio of product mixture/HCl aq./Et_2O = 1:5:5 (v/v/v) was used. The organic phases were then repeatedly dried with sodium sulfate, filtered and concentrated via rotary evaporation (T = 40 °C, p = 10 mbar). The obtained white-brown solid powders were combined and further dried in a vacuum oven (T = 40 °C, p = 5 mbar) before being used for biological conversion.

Compositional analysis of poplar biomass

Compositional analysis was performed following National Laboratory of the Rockies standard laboratory analytical procedure[56].

Elemental analysis of HDO lignin oil

Elemental analysis was performed following National Laboratory of the Rockies standard laboratory analytical procedure[57].

HPLC–DAD method for the quantitative analysis of the monomers in the RCF oil

Analysis of RCF products was performed using an Agilent 1290 series ultrahigh-performance liquid chromatography system with a diode array detector (UHPLC–DAD), upon calibration with standards. A detailed procedure is reported elsewhere[58].

Gas chromatography–mass spectrometry method for the qualitative analysis of the HDO oils

Samples were prepared by diluting 20 µl deoxygenated material in 1 ml acetone. Analysis was performed using an Agilent Technologies 7820A GC System outfitted with an HP-5MS Ultra Inert 30 m × 250 µm × 0.25 µm column and an Agilent 5977B single quadrupole mass spectrometer detector. During analysis, 1 µl samples were manually injected into the gas chromatography–mass spectrometer, which used a method with a split ratio of 10:1, a split flow of 12 ml min^{-1} and an inlet temperature of 300 °C. The oven was programmed to ramp, after an initial hold (1 min), from 50 °C to 300 °C at a rate of 5 °C min^{-1} and held at 300 °C for 10 min (total run time of 61 min).

Gas chromatography–flame ionization detection method for the quantitative analysis of the monomers in the HDO oil

Samples were prepared by dilution of 1–10 mg deoxygenated material in 1 ml acetone. Analysis was performed using an Agilent Technologies 8890 GC System outfitted with an HP–5MS Ultra Inert 30 m × 250 µm × 0.25 µm column and a flame ion detector held at 300 °C, run in a splitless configuration with a column flow of 0.97 m min^{-1} helium. During analysis, 1 µl of each sample was injected via an Agilent 7693A Autosampler to the inlet held at a temperature of 350 °C. The oven was programmed to ramp, after an initial hold (1 min), from 50 °C to 140 °C at a rate of 5 °C min^{-1}, held for 1 min, ramped again to 310 °C at a rate of 25 °C min^{-1}, and held again for 1 min before method termination (total run time of 27.8 min).

UHPLC–DAD quantification of aromatic acid monomers after autoxidation

Monomer quantification of the three benzene tricarboxylic acids, three benzene dicarboxylic acids (phthalic acids), benzoic acid and biphenyl-3,3′ dicarboxylic acid was performed using the chromatographic conditions described elsewhere[59]. In brief, analysis performed using an Infinity II 1290 UHPLC system (Agilent Technologies) equipped with a G7117A DAD and coupled with a Zorbax Eclipse Plus C18 Rapid Resolution HD (2.1 × 50 mm, 1.8 µm) column. A gradient of 20-mM phosphoric acid and methanol was used to achieve separation of desired analytes. All compounds were analysed at a wavelength of 240 nm.

HSQC NMR analysis of the RCF and HDO oils

The sample was prepared by dissolving 100 mg of material in 500 µl acetone-d_6. The spectrum was acquired on a Bruker Avance Neo 500 MHz equipped with a 5-mm liquid-nitrogen Prodigy broadband observe cryoprobe using the pulse sequence hsqcedetgpsisp2.3. A Bruker TopSpin 4.1.1 was used for spectral processing. The central solvent peaks were used as references. The spectrum was processed using squared cosine-bell apodization in frequency 1 (F1) and matched Gaussian apodization in frequency 2 (F2) (line broadening [LB] = −0.1 Hz, Gaussian broadening [GB] = 0.001).

HSQC NMR analysis of the autoxidation mixture

The two-dimensional NMR spectrum was obtained using a Bruker AVANCE 400 NMR spectrometer equipped with a CryoProbe. Approximately 60 mg of the sample was dissolved by adding 0.6 ml dimethyl sulfoxide (DMSO)-d_6. The calibration of the chemical shifts was performed based on the DMSO peak cross-signal at δ_C/δ_H 39.5/2.49 ppm. The spectrum was processed using squared cosine-bell apodization in F1 and matched Gaussian apodization in F2 (LB = −0.1 Hz, GB = 0.001). For the autoxidation mixture, the cross-peaks reflected on the spectra were assigned based on literature data[60–63]. As expected, the presence of benzoic acid and other aromatic carboxylic acids is confirmed by the signals in the region δ_H/δ_C = 7.25–8.5/126–134 ppm. The presence of other aromatic species in lower concentration is suggested by the weak signals at δ_H/δ_C = 7.25–8.5/120–126 ppm. Partially oxygenated compounds, such as ketones and acetylated/non-acetylated alcohols are present in small amounts, as suggested by the peaks found in the oxygenated aliphatic region. Clear signals in the aliphatic region at δ_H/δ_C = 1.8–2.1/18–21 ppm referred to acetyl groups in esterified structures confirm that acetylated species are found in the isolated autoxidation mixture at a concentration of about 1.5%. These species were not quantified and not included in the monomer yields evaluated via HPLC.

Diffusion-ordered spectroscopy NMR analysis of the HDO oil and autoxidation mixture

Samples were prepared by dissolving 0.1 mg of substrate in 0.6 ml DMSO-d_6. Diffusion-ordered spectroscopy (DOSY) NMR data were collected on a 600-MHz Bruker AV4 NEO NMR spectrometer equipped with a 5-mm Bruker BBFO iProbe, which has a 5.05 G cm^{-1} maximum gradient strength. The bipolar stimulated echo method (ledbpgp2s Bruker pulse sequence) was utilized[64]. DOSY experimental parameters included 16 scan averages, 32 gradient steps, a diffusion delay (Δ) of 70 ms and a total gradient pulse duration (δ) of 3 ms (corresponding to a gradient pulse P30 = 1,500 µs per lobe in the bipolar gradient pair). Data were processed using MestreNova (MNova) version 15. All individual DOSY points were phased and baseline corrected, then diffusion coefficients were extracted using MNova's DOSY transform module using the 'Peak Fitting' option.

Gel permeation chromatography of the RCF lignin oil

Gel permeation chromatography was conducted as reported elsewhere[65]. In brief, samples were prepared for gel permeation chromatography first by acetylation of 10–20 mg substrate in 0.5 ml pyridine and 0.5 ml acetic anhydride at 40 °C for 24 h under stirring. Subsequently, 1 ml aliquots of methanol were then added to each sample and dried under N_2, repeated 5 times. Samples were then dissolved in tetrahydrofuran, stirred for 30 min and filtered through a 0.2-µm polytetrafluoroethylene syringe filter. Twenty microlitres of each sample was injected on a HPLC equipped with 3 Agilent 7.5 × 300 mm PLgel gel permeation chromatography columns (10 µm × 50 Å, 10 µm × 10^3 Å, and 10 µm × 10^4 Å) in series. Tetrahydrofuran was utilized as a carrier solvent at an isocratic 1 ml min^{-1} for 40 min. Analytes were monitored via an ultraviolet DAD at a wavelength of 260 nm with a reference wavelength of 550 nm.

Preparation of commercial substrates and autoxidation substrate for bioconversion

Individual stocks of benzoate, phthalate, terephthalate, isophthalate, 1,2,4-benzene tricarboxylic acid (1,2,4-BTA), 1,2,3-BTA and 1,3,5-BTA were prepared at 100 mM (benzoate, phthalate, isophthalate and terephthalate) or 80 mM (1,2,4-BTA, 1,2,3-BTA and 1,3,5-BTA) by adding deionized water to the appropriate mass of commercial substrates and solubilizing by slowly raising the pH to about 7.5 with 4-N NaOH. A 125-mM stock of biphenyl-3,3′-dicarboxylic acid (B33DA) was prepared in DMSO. Autoxidation substrate was prepared for bioconversion in shake flasks by dissolving the substrate at 100 g l^{-1} in water and slowly raising the pH to 7 with sodium hydroxide. A 1,000× trace-metals solution was prepared by dissolved the following in water: 0.5 g l^{-1} Na_4EDTA (EDTA is ethylenediaminetetraacetic acid), 2 g l^{-1} $FeCl_3$, 0.05 g l^{-1} each H_3BO_3, $ZnCl_2$, $CuCl_2{\cdot}2H_2O$, $MnCl_2{\cdot}4H_2O$, $(NH_4)_2MoO_4$, $CoCl_2{\cdot}6H_2O$, $NiCl_2{\cdot}6H_2O$ and 1 m l^{-1} concentrated HCl. Stocks were sterilized by 0.2-µm filtration before biological cultivations.

Enrichments and isolation for phthalate-catabolizing bacteria from the environment

A soil sample was added to 25 ml mM9-En minimal medium (6 g l^{-1} Na_2HPO_4, 3 g l^{-1} KH_2PO_4, 0.5 g l^{-1} NaCl, 10 mM $(NH_4)_2SO_4$, 2 mM $MgSO_4$, 100 µM $CaCl_2$, 18 µM $FeSO_4$ and 1× trace metals, 0.2 mg l^{-1} biotin and 0.2 mg l^{-1} thiamine, pH 7.0) supplemented with 20 mM phthalate as a sole carbon source in a 125-ml Erlenmeyer flask, and incubated at 30 °C, 220 rpm. After 72 h, the culture became turbid. Two per cent of this culture was propagated to a clean 125-ml flask with 25 ml mM9-En + 20 mM phthalate and incubated for an additional 24 h. This outgrowth was then streaked for single colonies on mM9-En + 20 mM phthalate agar plates (15 g l^{-1} agar) and incubated at 30 °C. Two single colonies were picked into 5 ml mM9-En + 20 mM phthalate in a 15-ml falcon tube and grown at 30 °C overnight. These cultures were designated AG8816 and AG8838. These cultures were used to create frozen glycerol (25%) cell stocks. The remaining volume of these cultures were centrifuged at 3,000*g*, and the supernatant was removed. The resulting cell pellets were used for whole-genome sequencing.

Isolation of genomic DNA

For AG8816 and AG8838, high-molecular-weight genomic DNA was extracted by a Qiagen HMW DNA Purification Kit (catalogue number 67563) using the Gram-negative extraction protocol. The genomic DNA was barcoded for Oxford Nanopore whole-genome sequencing using the SQKRBK004 Library Prep kit and then sequenced using a Flongle flow cell (FAL50017). Base calling was performed using Guppy, and reads were filtered using Filtlong. Nanopore reads were assembled de novo using Flye, and Racon and Mekada were used to polish the resulting assembly. The assembled genome was annotated using Prokka.

Reads were filtered using Filtlong to remove all reads shorter than 1,000 bps and to remove the worst 5% of reads with the flags '--min_length 1000 -p 95'. These reads were fed into the Trycycler[66] workflow together with the Flye[67], Raven[68] and minimap/miniasm[69] assemblers. Consensus sequences generated by the Trycycler workflow were then polished using Oxford Nanopore Technology's Medaka polisher.

Identification of candidate phthalate genes

A possible phthalate 4,5-dioxygenase was identified in the genome annotations for both AG8816 and AG8838. This was further supported by aligning the corresponding protein sequences with the *Comamonas* sp. E6 and *P. putida* NMH102 phthalate 4,5-dioxygenase (Supplementary Data 1). Similar alignments were used to identify protein sequences in the surrounding regions of AG8816 and AG8838 for the remaining enzymes of the phthalate degradation pathway. Two decarboxylase candidates were identified in both AG8816 and AG8838, dubbed OphC1 and OphC2. The latter lacked sequence similarity to the OphC candidates but was colocalized with the other genes of the phthalate pathway in AG8816.

Putative transport genes were also found in or adjacent to the *oph* operons in these organisms. A tripartite tricarboxylate transporter (TTT)-type solute binding protein was selected from the *Comamonas* sp. E6 and AG8838 phthalate operons. Major facilitator superfamily (MFS)-type transporters (OphK) were found in AG8816 and *P. putida* NMH102. In addition, a putative TRAP-TAXI-type transporter (where TRAP strands for tripartite ATP-independent periplasmic and TAXI stands for TRAP-associated extracytoplasmic immunogenicity protein), OpaNL, was also included from PTH10, a plasmid required for phthalate catabolism in *Pseudomonas* sp. strain PTH10[70]. Phthalate catabolism in PTH10 proceeds via hydroxylation at the 2 and 3 carbons of phthalate and does not yield protocatechuic acid, so its catabolic genes were not included in the multiplexed serine-recombinase-assisted genome engineering (mSAGE) pool.

All genes were codon optimized for expression in *P. putida* KT2440 using the SALIS lab operon expression optimization software[71–74]. The first gene of each operon was placed after JER01, a strong *P. putida* ribosome binding site (RBS)[75], and downstream genes affixed to RBS sequences generated by the operon expression optimization software. The genes of the transporter module were placed under $P_{JE151211}$, a medium strength promoter, while the catabolic genes were placed after P_{tac}, a strong promoter in *P. putida*[75]. These plasmids also included *attP* sites to enable mSAGE. Plasmids for phthalate catabolic module 1 (OphA2A2B) included a BXB1 *attP* site and *kanR*. Likewise, the plasmids for phthalate catabolic module 2 (OphC or OphC1C2) included an R4 *attP* site and *gmR* and the plasmids for the transport module included a TG1 *attP* site and *smR*. These plasmids were synthesized by Genscript USA (Supplementary Table 1). Promoter, RBS and protein sequences are listed in Supplementary Table 4.

Plasmid and strain construction

Plasmids, primers and strains used in this work are listed in Supplementary Tables 1–3, respectively. All primers were synthesized by Integrated DNA Technologies.

Strain construction via serine-recombinase-assisted genome engineering

Electrocompetent cells were electroporated with a serine-recombinase-assisted genome engineering (SAGE) cargo plasmid containing the operon of interest and a suicide vector expressing the corresponding integrase, as described previously[37]. After electroporation, cells were recovered in 1 ml Luria–Bertani (LB) medium and incubated at 30° C, 220 rpm, for 1 h. The recovery mixture was then plated on LB agar plates supplemented with the appropriate antibiotic (corresponding to the SAGE cargo plasmid(s)) and incubated at 30° C overnight. Single colonies were streaked an additional time on

LB agar + antibiotic(s) plates and the insertion of the SAGE cargo plasmid was confirmed using colony PCR with primers that bind to the *P. putida* KT2440 genome adjacent to the integration site. In the case of AG11118, to enable additional SAGE transformations, the *kanR* resistance marker and colE1 replicon were removed using PhiC31 integrase. In brief, electrocompetent cells were made from AG5577 transformed with pALC878, and transformed with pGW30[39]. This plasmid contains an apramycin resistance marker, a temperature-sensitive replicon for *P. putida*, and expresses phiC31 integrase. This integrase recombines PhiC31 *attP* and *attB* sites that flank the replicon and resistance marker of pALC878, removing them from the genome. After transformation and selection on LB agar + 50 mg l^{-1} apramycin (apr 50) plates, single colonies were incubated at 37 °C in LB medium. This culture was streaked for isolation on LB agar plates without antibiotic and incubated at 37 °C. Single colonies were then replated in parallel on LB agar plates without antibiotic, LB agar + 50 mg l^{-1} kanamycin plates, and LB agar + apr 50 plates to verify loss of kanamycin resistance and apramycin resistance, and thus, loss of the associated DNAs (pALC878 replicon-marker backbone and pGW30 plasmid). The recombination of PhiC31 *att* sites in the resulting strain, named AG11118, was confirmed by colony PCR using primers oDJP169 and oALC1123.

Strain construction via homologous recombination

Gene deletions, insertions and replacements were performed in *P. putida* KT2440 via homologous recombination with antibiotic selection/*sacB* counterselection as described previously[76]. Suicide plasmids (Supplementary Table 1) used for homologous recombination were constructed using NEBuilder HiFi DNA Assembly Master Mix, transformed into NEB 5-alpha F′*I*^{q} competent *E. coli* (high efficiency) cells, and sequence-confirmed via whole-plasmid sequencing by Plasmidsaurus. Plasmids were either transformed directly or transferred by conjugation into *P. putida* KT2440 strains targeted for engineering. For conjugation, we used *E. coli* WM6026 as donor cells. After transformation or conjugation of suicide plasmids into *P. putida* KT2440 strains, streaking and downstream sucrose counterselection was performed by following a previously published method[76].

To transform plasmids into *P. putida* KT2440 strains directly or into *E. coli* WM6026 donor cells, we made the cells electrocompetent by carrying out three steps. (1) We centrifuged the cells (4,000*g* for 5 min at 4 °C), removed the supernatant and resuspended them in equal volume of ice cold 300 mM sucrose solution (*P. putida* KT2440) or 10% glycerol (*E. coli* WM6026). (2) We repeated step 1 twice with half the volume of 300-mM sucrose (*P. putida* KT2440) or 10% glycerol (*E. coli* WM6026) solution. (3) We repeated step 1 but resuspended cells in 0.1 ml 300-mM sucrose (*P. putida* KT2440) or 10% glycerol (*E. coli* WM6026) solution (ice cold). Competent cells were electroporated with 300–500 ng of plasmid and recovered for 1.5 h at 30 °C (*P. putida* KT2440) or 37 °C (*E. coli* WM6026) with shaking at 225 rpm in 950 µl of SOC media (*P. putida* KT2440; SOC: 20 g l^{-1} tryptone, 5 g l^{-1} yeast extract, 10 mM NaCl, 2.5 mM KCl, 10 mM $MgCl_2$, 10 mM $MgSO_4$ and 20 mM glucose) or 950 µl of SOC media containing 300 µM diaminopimelic acid (DAP) (*E. coli* WM6026). After recovery, cells were plated on LB agar plates supplemented with 50 µg ml^{-1} kanamycin sulfate (*P. putida* KT2440) or 50 µg ml^{-1} kanamycin sulfate and 300 µM DAP (*E. coli* WM6026), and incubated overnight (or until colonies appeared) at 30 °C. Single colonies of transformed *P. putida* KT2440 were restreaked onto a new LB plate with 50 µg ml^{-1} kanamycin sulfate to purify transformed *P. putida* KT2440 cells from any remaining untransformed cells. Transformed donor *E. coli* WM6026 cells were used to transfer plasmids to *P. putida* KT2440 strains as described below.

To conjugate plasmids from the donor *E. coli* WM6026 strain to *P. putida* KT2440 strains, we performed the following steps. (1) We inoculated separate overnight cultures of the plasmid-containing donor *E. coli* WM6026 strain and the recipient *P. putida* KT2440 strain. The donor strain was incubated overnight in LB medium supplemented with 50 µg ml^{-1} kanamycin sulfate and 300 µM DAP at 37 °C and 225 rpm. The recipient strain was incubated overnight in LB medium at 30 °C and 225 rpm. (2) We centrifuged 0.5 ml of both donor and recipient cells from the overnight cultures separately at 5,000*g* for 2 min and washed the cells twice in LB medium to remove any antibiotic. We resuspended the pellets in 0.5 ml LB medium supplemented with 300 µM DAP, combined the resuspended pellets and centrifuged again. We then resuspended the mixed cell pellet in 50 µl LB medium and dropped the mixture onto a LB plate supplemented with 5 µg ml^{-1} kanamycin sulfate and 30 µM DAP. The plate was incubated overnight at 30 °C to allow for conjugation. (3) Next, we scraped cells from the plate, resuspended them in 200 µl LB medium and plated them onto an LB plate supplemented with 50 µg ml^{-1} kanamycin sulfate. The plate was incubated at 30 °C overnight. (4) Single colonies were restreaked onto a new LB plate with 50 µg ml^{-1} kanamycin sulfate to purify conjugated *P. putida* cells away from any remaining non-conjugated *P. putida* cells or *E. coli* WM6026 donor cells.

After the second streak on LB plates containing 50 µg ml^{-1} kanamycin, counterselection on YT-sucrose (10 g l^{-1} tryptone, 5 g l^{-1} yeast extract, 250 g l^{-1} sucrose and 18 g l^{-1} agar) plates was performed to ensure removal of the plasmid backbone from the *P. putida* KT2440 genome. Diagnostic colony PCR with MyTaq HS Red Mix (Bioline) or Q5 Hot Start High-Fidelity 2X Master Mix (NEB) and primers listed in Supplementary Table 2 was utilized to confirm all gene deletions, insertions and replacements (Supplementary Table 3). Purified linear amplicons were sequence-confirmed by Plasmidsaurus. Confirmed strains were glycerol stocked and stored at −80 °C for future use.

Generation and outgrowth of the AG11118 mSAGE library

mSAGE cargo plasmids (pALC861-pACL870 and pALC874-878) were pooled together to a final concentration of 100 ng $µl^{-1}$, split equally by mass between each plasmid in the pool. Similarly, integrase-expressing suicide vectors (pGW031, pGW032, pGW038 and pGW039) were pooled to a final concentration of 1,000 ng $µl^{-1}$, split evenly between each integrase. AG11118 competent cells were transformed by mixing 100 µl of competent cells with 100 ng of the pooled SAGE cargo mixture and 1,000 ng of the pooled integrase cargo mixture and electroporating with a Gene Pulser Xcell Microbial electroporation system (Bio-Rad). Cells were recovered by resuspension in 900 µl LB and incubated for 1 h at 30 °C, 220 rpm. This transformation was repeated five times in parallel. After recovery, 5% of the recovery solution was plated on LB agar plates containing four antibiotics (50 mg l^{-1} kanamycin, 15 mg l^{-1} gentamycin, 200 mg l^{-1} spectinomycin and 300 mg l^{-1} streptomycin). From this plating, the mSAGE transformant library was calculated to be 200 colony-forming units (CFU; 200 transformants with both catabolic modules and a transport module). The remaining recovery for each of the 5 transformations was then pooled and split between three 250-ml Erlenmeyer flasks containing 50 ml LB with the previously mentioned antibiotics, and grown overnight at 30 °C, 220 rpm. One per cent of this culture was then transferred to 50 ml mM9 medium (6 g l^{-1} Na_2HPO_4, 3 g l^{-1} KH_2PO_4, 0.5 g l^{-1} NaCl, 10 mM $(NH_4)_2SO_4$, 2 mM $MgSO_4$, 100 µM $CaCl_2$, 18 µM $FeSO_4$ and 1× trace metals, pH 7.0) + 20 mM of *p*-coumarate and grown overnight. For each of the three flasks, 10 µl of this culture was added to 2 wells of a Greiner Bio-one 48-well plate containing 490 µl mM9 + 10 mM phthalate and incubated in an Epoch2 plate reader (540 double orbital shaking, 30 °C). After 120 h of growth, only 1 of 6 replicates showed growth. Ten microlitres of this isolate was transferred into 490 µl mM9 + 10 mM phthalate and grown in a Greiner Bio-one 48-well plate incubated in the Epoch2 plate reader (540 double orbital shaking, 30 °C). This outgrowth was streaked on an LB agar plate, and three isolated colonies were saved as frozen glycerol stocks: ALC701, ALC702 and ALC703.

Freezer stocks of strains ALC701-703 were streaked onto LB agar plates and incubated at 30 °C overnight. Isolated colonies were transferred into 3 ml LB media and grown overnight at 30 °C, 220 rpm. One

per cent of this culture was used to inoculate 3 ml mM9 media + 20 mM of *p*-coumarate and grown overnight at 30 °C, 220 rpm. Ten microlitres of each preculture was added to 490 µl mM9 media + 10 mM phthalate in a Greiner Bio-one 48-well plate. The plate was incubated in an Epoch2 plate reader (540 double orbital shaking, 30 °C) and optical density was measured to evaluate cell growth (Supplementary Fig. 17b). ALC703 was the fastest-growing isolate and was renamed AG11808. Whole-genome sequencing was performed on a cell pellet of AG11808 by Plasmidsaurus. The *ophC1C2* genes from AG8816 and the dioxygenase module from *Comamonas* E6 were found intact at the expected sites in the genome of AG11808. Interestingly, the transport module from AG8816 was observed in AG11808, but with the promoter mutated from JE151211 to become identical to P_{tac} (ref. 75). The nucleotide sequence of these promoters differs by only 4 bases spread across a 24-base-pair region. This 24-base-pair region is flanked upstream by 155 bases and downstream by 74 bases of sequence that match the mSAGE cargo plasmids for the other 2 modules, both of which contain the P_{tac} promoter. Thus, it is likely that this promoter change is a result of a homologous recombination-based gene conversion event rather than independent mutation of these four bases.

Fourty-eight-well plate cultivations

Freezer stocks of each strain were streaked onto LB agar plates and incubated at 30 °C overnight. Isolated colonies were picked into 3 ml LB media and grown overnight at 30 °C, 220 rpm. One per cent of this culture was then transferred to 3 ml mM9 + 20 mM of *p*-coumarate and grown overnight. From this preculture, 10 µl was added to a Greiner Bio-one 48-well plate containing 490 µl mM9 + 10 mM phthalate. This plate was incubated in an Epoch2 plate reader (540 double orbital shaking, 30 °C) and optical density at 600 nm (OD_{600}) was measured to determine cell growth.

BioscreenC microtitre plate cultivations

Microtitre plate cultivations were used to calculate lag times and growth rates for strains in this study. To prepare cells for microtitre plate cultivations, precultures of engineered *P. putida* KT2440 strains were inoculated into LB broth (Miller) from glycerol stocks and grown overnight at 30 °C and 225 rpm. Cells were washed with 1× M9 salts and inoculated into M9 minimal medium (6.78 g l^{-1} Na_2HPO_4, 3 g l^{-1} KH_2PO_4, 0.5 g l^{-1} NaCl, 1 g l^{-1} NH_4Cl, 2 mM $MgSO_4$, 100 µM $CaCl_2$ and 18 µM $FeSO_4$, pH 7.0) containing the desired carbon source, as specified, at an OD_{600} of 0.1 in triplicate. Cells were cultivated in 200 µl volume in a Honeycomb 100-well plate at 30 °C with maximum orbital shaking. Growth was measured in a BioscreenC (Growth Curves) at 600 nm absorbance with 15-min read intervals.

Shake-flask cultivations

Precultures were prepared by inoculating engineered *P. putida* KT2440 strains into LB broth (Miller) from glycerol stocks and were grown overnight at 30 °C and 225 rpm. Cells were washed with 1× M9 salts and inoculated, in triplicate, into 30 ml M9 minimal medium (described above) containing the desired carbon source, as specified, at an OD_{600} of 0.1. Cells were cultivated in 125 ml baffled Erlenmeyer flasks with metal caps at 30 °C and 225 rpm in a benchtop incubator (0.75″ orbital). Growth was measured via OD_{600} using a 1:10 dilution. To sample for metabolite analysis, 1 ml of culture was removed, centrifuged for 2 min at >18,000*g* and filtered (0.2-µm syringe filter) into amber glass vials. A 10× dilution and 50× dilution in water and 1× M9 salts was required for aromatic and muconolactone analysis, respectively. Samples were stored at −20 °C before analysis.

Adaptive laboratory evolution

The adaptive laboratory evolution (ALE) was carried out in a Biotek LogPhase 600 Microbiology Reader (BioSPX), referred to hereafter as LP600. AW521, an engineered *P. putida* KT2440 strain (this study) was used as a parent strain for the ALE experiment. To initiate the ALE, a preculture of AW521 was prepared as described above. Cells from the preculture were washed with 1× M9 salts and were inoculated (with 6 replicates) into M9 minimal medium supplemented with 10 mM phthalic acid at an OD_{600} of 0.1. Cells were cultivated in 200 µl volume in a Thermo Scientific Nunc Edge 96-well, non-treated, flat-bottom microplate at 30 °C (gradient mode) at 500 rpm. Growth was measured in the LP600 instrument at 600 nm absorbance with 20-min read intervals. Cells were transferred serially into fresh growth media at the end of the exponential phase to maintain selection pressure: that is, when OD_{600} reached about 0.8 (OD_{600} < 1), 12.5% (v/v) inoculum size was propagated into a freshly filled well with M9 minimal medium supplemented with 10 mM phthalic acid. Throughout the ALE, 6 independent replicates for AW521 were evolved over 6 serial passages and approximately 15 days.

For each ALE lineage, the endpoint population and one endpoint isolate were selected and prepared for whole-genome sequencing. Isolates were selected by streaking populations onto M9 agar supplemented with 10-mM phthalate. Isolates and populations were inoculated into 10 ml M9 minimal medium supplemented with 10-mM phthalate and grown at 30 °C and 225 rpm until an OD_{600} of about 1 was reached. Cells were pelleted by centrifuging at 5,000*g* for 5 min, washed with 1 ml PBS (137 mM NaCl, 2.7 mM KCl, 4.3 mM Na_2HPO_4, pH 7.4) and resuspended in DNA/RNA Shield Reagent (Zymo Research). Resuspended pellets were submitted to Plasmidsaurus for genomic DNA extraction and whole-genome sequencing (Oxford Nanopore long reads). Geneious Prime version 2023.0.2 was used to align sequencing reads (medium sensitivity/fast; 5 iterations), construct consensus sequences, and call SNPs. To call SNPs, the following settings were used: minimum coverage of 10 reads, maximum variant frequency of 65%, maximum variant *P* value of 10^{-6}, minimum strand-bias *P* value of 10^{-5} when exceeding 65% bias, and a default genetic code of standard. Raw sequencing reads are available on NCBI BioProject PRJNA1289884; BioSample and Sequence Read Archive information are available in Supplementary Data 1.

Growth parameter calculations

To determine growth parameters for our bacterial strains, we fit growth curves to a single-Gompertz model with the following equation:

$$y = A e^{-e^{\frac{\mu_A e}{A}(\lambda - t)+1}} + C,$$

where y is the OD_{600} reading, A is the upper asymptote (OD_{600} units), μ_A is the absolute growth rate (Mu; OD_{600} h^{-1} units), t is time in hours (h units), λ is the lag time (h units) and C is the lower asymptote (OD_{600} units).

Bioreactor cultivations

The bioconversion of the autoxidation substrate or mock mixture to muconolactone was performed by *P. putida* KMM0037 using a DO-stat-fed-batch strategy, based on a modified protocol from our previous work[77], or a fed-batch strategy at constant feed rates.

For the seed of all bioreactor campaigns, a scrape of a frozen glycerol stock was used to inoculate 50 ml LB Miller media in independent 250-ml baffled flasks. The cultures were incubated 16–18 h at 30 °C at 225 rpm. Then the cells were centrifuged at 4,600*g* for 5 min, the supernatant was removed and the cells were resuspended in 5 ml modified M9 medium (see below). The resuspended cells were used to inoculate the bioreactors to an initial OD_{600} of 0.2. For the bioreactor experiments, OD_{600} was measured using a nanodrop (Thermo Scientific).

P. putida KMM0037 was cultivated in 0.5-l BioStat-Q Plus bioreactors (Sartorius Stedim Biotech) containing 200 ml modified M9 medium with 2.7 g l^{-1} (15 mM) of glucose, 13.56 g l^{-1} Na_2HPO_4, 6 g l^{-1} KH_2PO_4, 1 g l^{-1} NaCl, 2.25 g l^{-1} $(NH_4)_2SO_4$, 2 ml l^{-1} of 1 M $MgSO_4$ solution, 0.1 ml l^{-1} of 1 M $CaCl_2$ solution, 2 ml l^{-1} of 5 g l^{-1} $FeSO_4 \times 7H_2O$ solution, and 1 ml l^{-1} antifoam 204 (A6426; Sigma-Aldrich). The cultivations were maintained at 30 °C, 7.0 pH using 4 M NaOH, and sparged with air at 1.5 vvm. The initial

agitation in the batch phase was set at 350 rpm. Once the saturation of oxygen reached 30%, the DO was maintained at 30% by automatic agitation changes using a DO cascade with a 5% dead band. When the glucose was depleted, the DO increased to 75%, at which point the fed-batch phase was initiated. In the batch phase, 4 h after inoculation, 0.844 ml of a filter sterilized (0.2 µm; Nalgene PES) solution of 13.2 g l^{-1} phthalic acid, 2.8 g l^{-1} terephthalic acid, 7.3 g l^{-1} isophthalic acid and 42.9 g l^{-1} benzoic acid (pH 8.1) was added to reach a concentration of 2 mM in the bioreactor. The mock lignin solution was used for induction in all bioreactor experiments, even when autoxidation substrate was used for the latter fed-batch phase.

The fed-batch phase with autoxidation substrate and mock autoxidation substrate was first conducted using a DO-stat-fed-batch strategy. The autoxidation substrate feed contained 100 g l^{-1} of autoxidation substrate (prepared by weight and solubilized in water by neutralizing the mixture to pH 8.1 with 10 M NaOH), 85.4 g l^{-1} glucose, 12 g l^{-1} ammonium sulfate and 4 ml l^{-1} antifoam 204. The feed for the autoxidation substrate mock mixture was made from commercially available aromatic compounds and contained 13.2 g l^{-1} phthalic acid, 2.8 g l^{-1} terephthalic acid, 7.3 g l^{-1} isophthalic acid, 42.9 g l^{-1} benzoic acid, 3.8 g l^{-1} 1,2,4-BTA, 1.8 g l^{-1} 1,2,3-BTA, 0.42 g l^{-1} 1,3,5-BTA, 1.3 g l^{-1} B33DA, 85.4 g l^{-1} glucose, 12 g l^{-1} ammonium sulfate and 4 ml l^{-1} antifoam 204 (A6426; Sigma-Aldrich). Unless otherwise stated, all experiments with the mock mixture were conducted with this feed composition containing 1:1 molar concentration of bioavailable aromatics/glucose, where the bioavailable aromatics were phthalic acid, terephthalic acid, isophthalic acid and benzoic acid, specifically. For a set of duplicate bioreactor cultivations, we tested a feed with a 1:0.5 molar concentration of bioavailable aromatics: glucose. This feed was composed of 13.2 g l^{-1} phthalic acid, 2.8 g l^{-1} terephthalic acid, 7.3 g l^{-1} isophthalic acid, 42.9 g l^{-1} benzoic acid, 3.8 g l^{-1} 1,2,4-BTA, 1.8 g l^{-1} 1,2,3-BTA, 0.42 g l^{-1} 1,3,5-BTA, 1.3 g l^{-1} B33DA, 42.7 g l^{-1} glucose, 12 g l^{-1} ammonium sulfate and 4 ml l^{-1} antifoam 204 (A6426; Sigma-Aldrich). All mock mixture feeds were also adjusted to a pH of 8.1 with NaOH (10 M). Both autoxidation substrate and mock feeds were filter sterilized (0.2 µm; Nalgene PES) after neutralization. The feed was dosed for 30 s at a rate of 0.84 ml min^{-1} to target 1 mM bioavailable aromatics concentration in the bioreactor in each pulse. The feed was automatically added every time the DO reached 75%. The agitation was manually adjusted to maintain a minimum DO of approximately 20% (Supplementary Figs. 27–29, 34 and 36).

Autoxidation substrate and mock autoxidation substrate were also fed using constant feeding. Feeds were prepared as described above. The feed was set at 4 mM h^{-1}, 6 mM h^{-1} and 12 mM h^{-1} concentration of bioavailable aromatics for mock autoxidation substrate and 6 mM h^{-1} concentration of bioavailable aromatics only for autoxidation substrate, based on the initial working volume (200 ml) in the batch phase. Feeding rates of 4 mM h^{-1}, 6 mM h^{-1} and 12 mM h^{-1} were equivalent to a feed rate of 1.69 ml h^{-1}, 2.53 ml h^{-1} and 5.06 ml h^{-1}, respectively. In the fed-batch phase, DO was maintained at 30% by automatic agitation changes using a DO cascade with a 5% dead band. The experiments ended when the cultures died, as indicated by a rise in DO to >80% or a rapid decline in OD_{600}.

The spent broth from the autoxidation substrate case was centrifuged at 20,000*g* and 30 min, filtered through 0.2-µm pore-size membranes (0.2 µm, Nalgene PES) and used for further downstream separations.

Productivity and yield calculations in bioreactors. For all bioreactor cultivations productivity and yield were calculated using the following equations:

$$\text{Yield (mol\%)} = \frac{\text{Concentration of muconolactone (mol)}}{\text{Concentration of bioavailable aromatics fed (mol)}} \times 100\%$$

$$\text{Productivity (g l}^{-1}\text{ h}^{-1}\text{)} = \frac{\text{Concentration of muconolactone (g l}^{-1}\text{)}}{\text{Time after inoculation (h)}}$$

Analysis of aromatic substrates after autoxidation and biological product by UHPLC–mass spectrometry and mass spectrometry–DAD

Quantitation of the aromatic acid products after autoxidation and the biological product, muconolactone, and co-products, muconic acid isomers, catechol and protocatechuic acid required an alternative method than the one previously described here for the post autoxidation products owing to co-elution of some of the BTAs with the co-products and the lack of ultraviolet activity of muconolactone. UHPLC–mass spectrometry and mass spectrometry–DAD was utilized to alleviate these limitations. Method parameters were previously reported in detail[78]. In brief, samples were run on an Agilent Infinity II 1290 UHPLC system equipped with an Agilent 6475A triple quadrupole mass spectrometer. The mass spectrometer was run in negative mode using multiple reaction monitoring for quantitation of muconolactone. Chromatographic separation of all analytes was achieved utilizing a gradient of water and methanol, both containing 0.1% formic acid and 5 mM ammonium formate, and a BEH C18 column. The remaining analytes of interest were quantitated using responses from the DAD at either 240 nm or 265 nm depending on the analyte.

Quantitation of glucose and small acids in biological cultivation samples

Glucose and small aliphatic co-products were analysed by HPLC as previously detailed[79]. In brief, samples and standards were injected onto an Aminex HPX-87H column (Bio-Rad) and eluted using an isocratic mobile phase of 0.01 N sulfuric acid in water. A refractive index detector was utilized for detection and quantitation.

Isolation of muconolactone from bioreactor cultivations

Spent broth was acidified to pH 2 with concentrated HCl. The product was extracted with ethyl acetate (3 × 100 ml) and the organic phase was dried over Na_2SO_4. Acetic acid (1%) was added to the solution and then passed through a silica plug. The solution was concentrated to dryness by rotary evaporation, followed by drying under high vacuum to obtain an orange solid. We note that owing to impurities in the product, we did not utilize this material to make adipic acid or dimethyl β-ketoadipate described below.

Synthesis of muconolactone methyl ester

Purified muconolactone (1 equivalent; prepared and purified in house as described previously)[43] was refluxed in methanol with Amberlyst-15 for 16 h. The solid catalyst was filtered and the methanol was removed by rotary evaporation. The solid was purified by column chromatography (0–50% hexane/ethyl acetate gradient), to yield muconolactone methyl ester.

^{1}H NMR spectroscopy ($CDCl_3$, 400 MHz) 7.60 (dd, J = 5.7, 1.6 Hz, 1H), 6.18 (dd, J = 5.7, 2.0 Hz), 5.40 (tt, J = 7.1, 1.8 Hz), 3.75 (s, 3H), 2.88 (dd, J = 16.5, 7.1 Hz, 1H), 2.64 (dd, J = 16.5, 7.1 Hz, 1H).

Synthesis of adipic acid from muconolactone methyl ester

Muconolactone methyl ester (1 equivalent) and K_2CO_3 (1.2 equivalents) were combined in water (10 ml) and stirred for 16 h. Quantitative conversion of muconolactone to potassium methyl muconate was confirmed by ^{1}H NMR spectroscopy in DMSO-d_6 (Supplementary Fig. 40). The yellow, aqueous solution was transferred to a 50-ml Parr reactor equipped with a stirrer bar, to which Pd/C (10 wt%) was added. The Parr was flushed with 30 bar of N_2, then pressurized with 5 bar of H_2. The reaction was run at ambient temperature (about 22 °C) for 3 h. The catalyst was removed by filtration (0.2 µm) and an aliquot was analysed by ^{1}H NMR spectroscopy to confirm saturation of the product to make

potassium methyl adipate (Supplementary Fig. 41). Finally, the methyl ester was hydrolysed with 1 equivalent of K_2CO_3, then acidified to pH 2 with concentrated HCl. The solution was concentrated to dryness then re-dissolved in acetone to remove KCl salts by filtration. The solution was evaporated in vacuo to yield adipic acid (99% yield by ^{1}H NMR spectroscopy, 88% isolated yield from pure muconolactone).

Synthesis of dimethyl β-ketoadipate from muconolactone methyl ester

Muconolactone methyl ester (150 mg, 0.96 mmol, 1 equivalent) and $Zn(OAc)_2$ (6 mg, 10 mol%) were combined in methanol (0.4 ml, 10 equivalents) in a microwave vial. The mixture was sealed with a crimp cap and heated to 100 °C for 12 h, reaching 90% conversion. The yellow solution was concentrated to dryness and the product was purified by column chromatography (0–60% hexane/ethyl acetate gradient) to yield a clear oil (176 mg, 0.86 mmol, 90% yield from pure muconolactone).

^{1}H NMR spectroscopy ($CDCl_3$, 400 MHz) 3.73 (s, 3H), 3.66 (s, 3H), 3.50 (s, 2H), 2.86 (t, J = 6.5 Hz, 2 H), 2.61 (t, J = 6.5 Hz, 2 H).

Data availability

Sequence data for environmental isolates and adaptive laboratory evolution populations and isolates are available on NCBI BioProject PRJNA1289884 (BioSample information listed in Supplementary Data 1). All other data from this study are included in the main text, Supplementary Information and Supplementary Data 1.

56. Sluiter, A. et al. *NREL/TP-510-42618: Determination of Structural Carbohydrates and Lignin in Biomass* (National Renewable Energy Laboratory, 2008).
57. Miscall, J., Christensen, E. D., Olstad, J., Deutch, S. & Ferrell, J. R. III *NREL/TP-5100-80967: Determination of Carbon, Hydrogen, Nitrogen, and Oxygen in Bio-oils* (National Renewable Energy Laboratory, 2021).
58. Woodworth, S. P., Ramirez, K. J. & Beckham, G. T. Aromatic monomers analysis for reductive catalytic fractionation of lignin by liquid chromatography with diode array detection. *protocols.io* https://doi.org/10.17504/protocols.io.bp2l6x6jdlqe/v1 (2025).
59. Haugen, S., Alt, H., Ramirez, K., Michener, W. E. & Beckham, G. T. Analysis of HDO autoxidation products by UHPLC-DAD. *protocols.io* https://doi.org/10.17504/protocols.io.kqdg31ex1l25/v1 (2026).
60. Hosseini-Sarvari, M., Ataee-Kachouei, T. & Moeini, F. Preparation, characterization, and catalytic application of nano Ag/ZnO in the oxidation of benzylic C–H bonds in sustainable media. *RSC Adv.* **5**, 9050–9056 (2015).
61. Gomez, M. V. & de la Hoz, A. NMR reaction monitoring in flow synthesis. *Beilstein J. Org. Chem.* **13**, 285–300 (2017).
62. Wang, Z. et al. Cooperative interplay between a flexible PNN–Ru(II) complex and a $NaBH_4$ additive in the efficient catalytic hydrogenation of esters. *Catal. Sci. Technol.* **7**, 1297–1304 (2017).
63. Zhang, Y. et al. Catalyst-free aerobic oxidation of aldehydes into acids in water under mild conditions. *Green Chem.* **19**, 5708–5713 (2017).
64. Wu, D. H., Chen, A. D. & Johnson, C. S. An improved diffusion-ordered spectroscopy experiment incorporating bipolar-gradient pulses. *J. Magn. Reson. A* **115**, 260–264 (1995).
65. Stanley, L., Katahira, R. & Beckham, G. T. Molecular weight determination of lignin via gel permeation chromatography. *protocols.io* https://doi.org/10.17504/protocols.io.n2bvj1r15vk5/v1 (2026).
66. Wick, R. R. et al. Trycycler: consensus long-read assemblies for bacterial genomes. *Genome Biol.* **22**, 266 (2021).
67. Kolmogorov, M., Yuan, J., Lin, Y. & Pevzner, P. A. Assembly of long, error-prone reads using repeat graphs. *Nat. Biotechnol.* **37**, 540–546 (2019).
68. Vaser, R. & Šikić, M. Time- and memory-efficient genome assembly with Raven. *Nat. Comput. Sci.* **1**, 332–336 (2021).
69. Li, H. Minimap and miniasm: fast mapping and de novo assembly for noisy long sequences. *Bioinformatics* **32**, 2103–2110 (2016).
70. Kasai, D. et al. 2,3-Dihydroxybenzoate meta-cleavage pathway is involved in *o*-phthalate utilization in *Pseudomonas* sp. strain PTH10. *Sci. Rep.* **9**, 1253 (2019).
71. Farasat, I. et al. Efficient search, mapping, and optimization of multi-protein genetic systems in diverse bacteria. *Mol. Syst. Biol.* **10**, 731 (2014).
72. Halper, S. M., Hossain, A. & Salis, H. M. Synthesis success calculator: predicting the rapid synthesis of DNA fragments with machine learning. *ACS Synth. Biol.* **9**, 1563–1571 (2020).
73. Reis, A. C. & Salis, H. M. An automated model test system for systematic development and improvement of gene expression models. *ACS Synth. Biol.* **9**, 3145–3156 (2020).
74. Cetnar, D. P. & Salis, H. M. Systematic quantification of sequence and structural determinants controlling mRNA stability in bacterial operons. *ACS Synth. Biol.* **10**, 318–332 (2021).
75. Elmore, J. R., Furches, A., Wolff, G. N., Gorday, K. & Guss, A. M. Development of a high efficiency integration system and promoter library for rapid modification of *Pseudomonas putida* KT2440. *Metab. Eng. Commun.* **5**, 1–8 (2017).
76. Johnson, C. W. & Beckham, G. T. Aromatic catabolic pathway selection for optimal production of pyruvate and lactate from lignin. *Metab. Eng.* **28**, 240–247 (2015).
77. Salvachúa, D. et al. Bioprocess development for muconic acid production from aromatic compounds and lignin. *Green Chem.* **20**, 5007–5019 (2018).
78. Ramirez, K., Ingraham, M., Haugen, S. & Beckham, G. T. Analysis of a lignin derived single product using chemical and biological redox using UHPLC-MS/MS-DAD. *protocols.io* https://doi.org/10.17504/protocols.io.36wgqprjyvk5/v1 (2026).
79. Alt, H. M. et al. Analysis of sugars, small organic acids, and alcohols by HPLC-RID. *protocols.io* https://doi.org/10.17504/protocols.io.5qpvob7y9l4o/v2 (2024).

Acknowledgements We thank M. L. Stone for a critical review of the paper and S. Lask for assistance in product quantification.

Author contributions Conceptualization: K.P.S., S.S.S., A.Z.W. and G.T.B. Methodology: K.M.M., C.T.P., D.R., M.S.W., G.R., A.L.C., N.R.M., K.J.R., K.P.S., A.M.G., D.S., Y.R.-L., S.S.S., A.Z.W. and G.T.B. Investigation: K.M.M., C.T.P., D.R., M.S.W., G.R., S.T.B., A.L.C., N.R.M., A.F.B, B.A.B., S.J.H., M.A.I., W.G.A., M.S., L.C.M., K.J.R. and A.Z.W. M.S.W. and L.C.M. performed the RCF reactions. M.S.W. performed the HDO reactions. C.T.P., D.R., M.S.W. and S.T.B. performed the autoxidation reactions. A.L.C. performed the phthalate catabolism bioprospecting. A.L.C, W.G.A. and M.S. genome-sequenced the phthalate-catabolizing bacterial isolates in this work. K.M.M., A.L.C., M.S. and A.Z.W. engineered the bacterial strains in this study. K.M.M. and A.L.C. performed small-scale bacterial cultivations and adaptive laboratory evolution. N.R.M. performed the bioreactor experiments. G.R. and B.A.B. performed conversion of muconolactone to adipic acid and dimethyl β-ketoadipic acid. A.F.B., S.J.H., M.A.I. and K.J.R. developed and performed analytical measurements. Visualization: K.M.M., C.T.P., D.R., M.S.W. and A.Z.W. Funding acquisition: A.M.G., D.S., Y.R.-L., S.S.S., A.Z.W. and G.T.B. Supervision: A.M.G., D.S., Y.R.-L., S.S.S., A.Z.W. and G.T.B. Writing—original draft: K.M.M., C.T.P., D.R., M.S.W., G.R., A.L.C., N.R.M., K.J.R., S.S.S, A.Z.W. and G.T.B. Writing—review and editing: all authors reviewed and approved the paper.

Funding This work was authored in part by the National Laboratory of the Rockies for the US Department of Energy (DOE) under contract number DE-AC36-08GO28308. This work was authored in part by Oak Ridge National Laboratory, which is managed by UT-Battelle, LLC, for the US DOE under contract DE-AC05-00OR22725. Funding to K.M.M., C.T.P., M.S.W., G.R., S.T.B., A.F.B., B.A.B., S.J.H., M.A.I., N.R.M., L.C.M., K.J.R., K.P.S., D.S., Y.R.-L., A.Z.W. and G.T.B. was provided by the US DOE Office of Critical Minerals and Energy Innovation Alternative Fuels and Feedstocks Office. For K.M.M., D.R., M.S.W., A.L.C., A.M.G., Y.R.-.L., A.Z.W. and G.T.B., this material is also based upon work at the Center for Bioenergy Innovation supported by the US Department of Energy, Office of Science, Biological and Environmental Research under contract number ERKP886. Contributions by S.S.S. were supported by the US Department of Energy, Office of Basic Energy Sciences, under award number DE-FG02-05ER15690. The views expressed in the article do not necessarily represent the views of the DOE or the US Government. The US Government retains and the publisher, by accepting the article for publication, acknowledges that the US Government retains a non-exclusive, paid-up, irrevocable, worldwide license to publish or reproduce the published form of this work, or allow others to do so, for US Government purposes.

Competing interests K.M.M., C.T.P., A.L.C., K.P.S., A.M.G., Y.R.-L., S.S.S., A.Z.W. and G.T.B. have filed a patent application on this concept (US provisional patent no U.S. 2024/0327877 A1).

Additional information

Supplementary information The online version contains supplementary material available at https://doi.org/10.1038/s41586-026-10580-x.

Correspondence and requests for materials should be addressed to Shannon S. Stahl, Allison Z. Werner or Gregg T. Beckham.

Peer review information *Nature* thanks Micaela Chacón, Neil Dixon and the other, anonymous, reviewer(s) for their contribution to the peer review of this work. Peer reviewer reports are available.

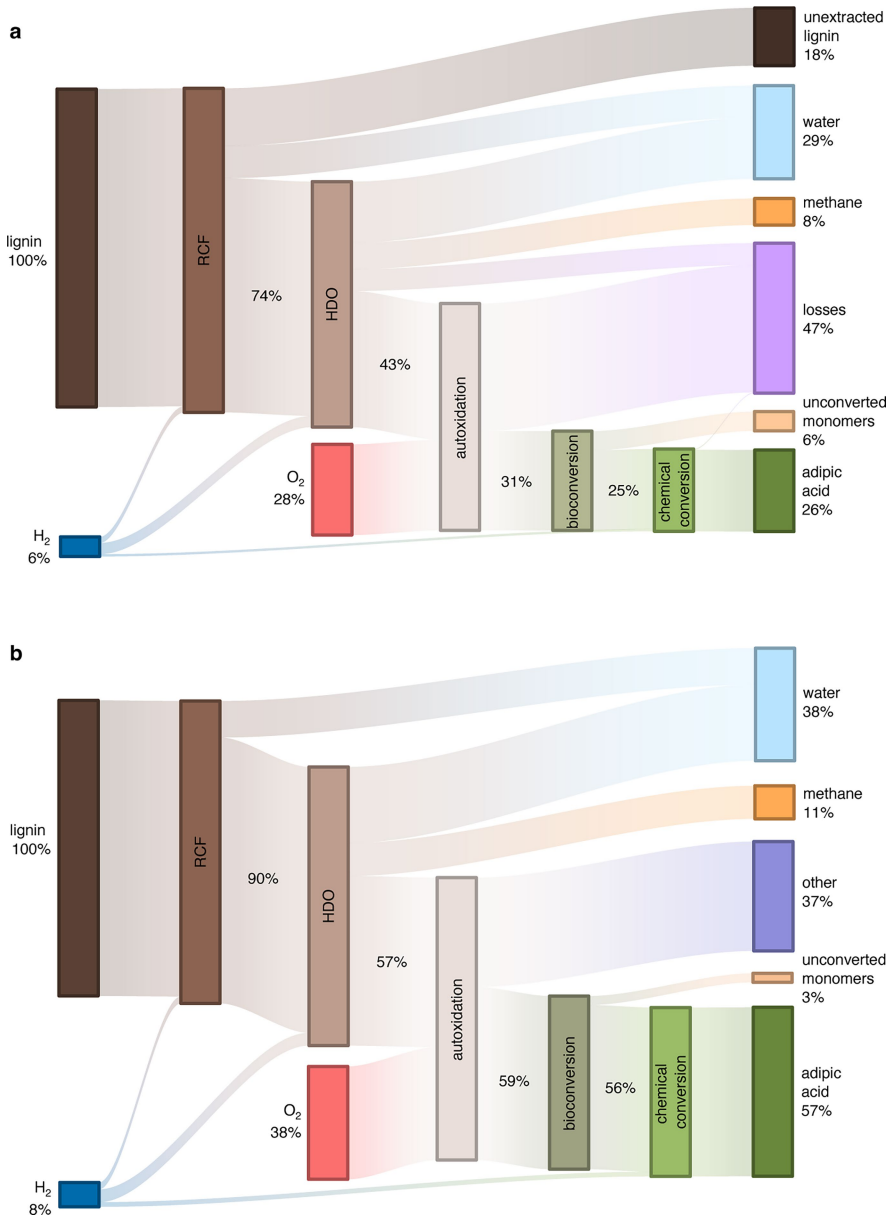

Extended Data Fig. 1 | Sankey diagrams showing the actual (a) and theoretical (b) mass yields of products through the overall process. (**a**) Mass yields were evaluated either gravimetrically or via analytical methods through the whole process as described in the experimental procedures section. Relevant assumptions have been detailed in the Supplementary text and Extended Data Fig. 2, while numerical values can be found in Data S1. (**b**) Calculation of theoretical process yields was performed as described in the Supplementary text. Calculations can be found in Data S1. Reaction conditions for RCF: 3 g poplar, 300 mg 5 wt% Ru/C, 30 mL MeOH/H_2O (2/1 v/v), 30 bar H_2, 225 °C, 700 rpm stirring, 3 h reaction time (not including ~30 min heat-up). Reaction conditions for HDO: poplar lignin RCF oil as the substrate, 8.6 g Mo_2C (60–100 mesh), 0.3 mL/min lignin oil, 270 mL/min H_2, 62 bar, 350 °C (first pass), 375 °C (second pass), and toluene at 3 mL/min for 30 min during start-up. Reaction conditions for autoxidation: 500 mg HDO lignin oil, 20 mL AcOH, 25 mg (5 wt%) $Co(OAc)_2{\cdot}4H_2O$, 25 mg (5 wt%) $Mn(OAc)_2{\cdot}4H_2O$, and 5 mg (1 wt%) NaBr (added from AcOH stock solutions of dissolved catalysts), 6 bar O_2, 220 °C, 3 h reaction not including heat-up time of ~0.5 h. Reaction conditions for bioconversion: KMM037 was cultivated in shake flasks (30 °C, 225 rpm) with 20 mM glucose and 10 mM aromatics from autoxidation substrate. Reaction conditions for muconolactone to adipic acid: 3 g muconolactone, 15 wt% Amberlyst-15, 50 mL MeOH, 68 °C, 16 h; 0.5 g muconolactone methyl ester, 1 equiv K_2CO_3, H_2O, RT, 16 h; 5 bar H_2, 50 mg Pd/C (5 wt% loading), H_2O, 22 °C, 3 h; 1 equiv K_2CO_3, H_2O, 70 °C.

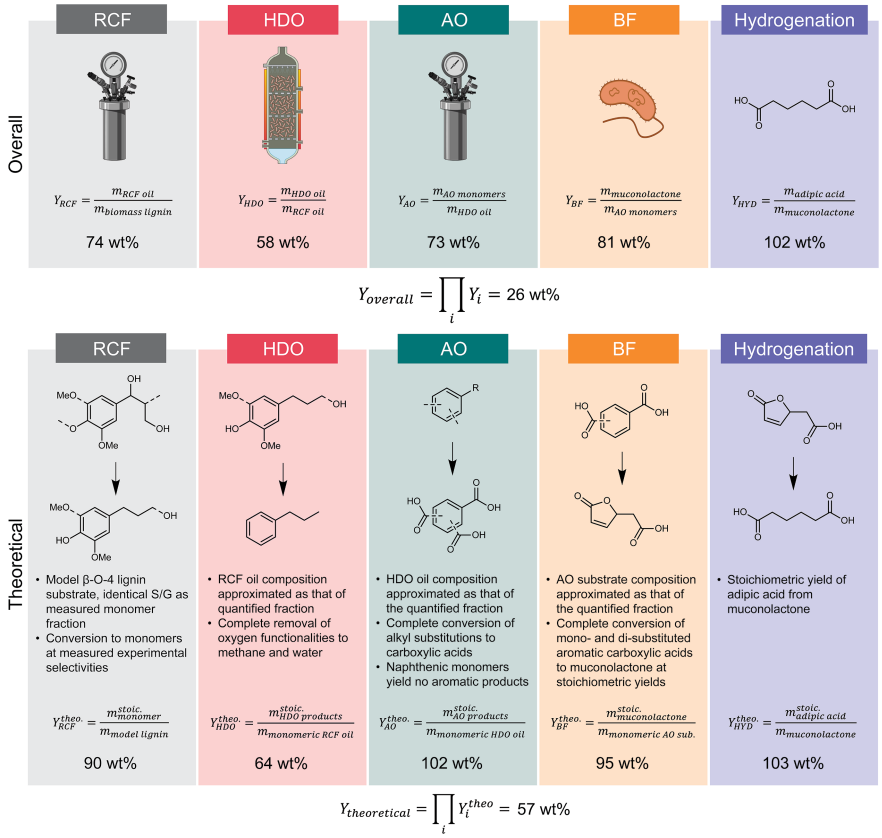

Extended Data Fig. 2 | Summary of yield equations used in determining stepwise process yields used to determine overall process yields reported in Fig. 1 and Extended Data Fig. 1. A more detailed explanation of yield calculations and assumptions can be found in the Supplementary text and Data S1. Abbreviations: RCF, reductive catalytic fractionation; HDO, hydrodeoxygenation; AO, autoxidation; BF, biological funneling; HYD, hydrogenation; Me, methyl; Y, yield; stoic, stoichiometric; theo, theoretical; sub, substrate. Figure created in BioRender; Mains, K. https://BioRender.com/9hcf8sw (2026).